

東京大学 大学院新領域創成科学研究科  
基盤科学研究系  
先端エネルギー工学専攻

平成 18 年度

修士論文

Developments of Polarity-Free  
Rectenna for Micro Aerial Vehicles

— マイクロ飛行機搭載用非偏波方向依存レクテナの開発 —

2007 年 2 月提出  
指導教員 小紫 公也 助教授

56206 勝永 健太

# Abstract

“Innovative Aerial Robot Project”(IARP) is a project for Unmanned Aerial Vehicle (UAV) and Micro Aerial Vehicle (MAV) which is carried out as part of the 21st century centers of excellence (COE) program, “Mechanical Systems Innovation”. “Innovative” means that MAV contains some challenging technologies. In this project, we plan to transmit microwave energy for MAV by phased array antenna. Since the yaw angle of flying MAV varies temporally, Making rectennas polarity-free is very important.

This paper reports development status of the polarity-free patch antenna for the receiving rectenna system. I designed and fabricated antennas, rectifier circuits, and rectennas, and measured their power conversion efficiencies. As a result I achieved near polarity-free antenna by Leaf MSA with its conversion efficiency of 36% on an average, 33% at a minimum, and 40% at a maximum. In addition, I developed the rectifier circuits with that of 14% at a maximum where the load resistance was  $250\Omega$ . Moreover, I produced a rectenna array consisted of four rectenna elements in parallel, and achieved to operating the electric motor for MAV.

In this experiment, we have constructed microwave transmission system. The microwave is provided by a 5.8GHz Field Effect Transistor (FET) microwave oscillator (Almotech Co.) and divided into five elements using a power divider. The phases of the microwave elements are controlled individually using two 6-bit phase shifters, whose phase resolution is 5.6deg. The phase shifters were controlled by a PC digitally. Three FET amplifiers with the output power of 0.7 watt each are used to have totally 3.5 watts output power. Each microwave is guided to each antenna. In this experiment, horn antenna is used in order to cut down the number of antenna. The power profile was obtained using a patch antenna connected with rectifier (Pasternack Co.) on a traverse stage.

# Table of Contents

## Abstract

<b>Chapter 1</b>	<b>Introduction.....</b>	<b>1</b>
<b>1.1</b>	<b>Power Supply System for Innovative Aerial Robot Project .....</b>	<b>1</b>
<b>1.2</b>	<b>Problems with MAV Circling .....</b>	<b>2</b>
1.2.1	Target Tracking .....	3
1.2.2	Effects of Pitch and Roll Angles .....	6
1.2.3	Effects of Yaw Angle .....	7
<b>1.3</b>	<b>Other Applications with Power Transmitting System.....</b>	<b>8</b>
<b>Chapter 2</b>	<b>Theory of Polarity-Free Antenna.....</b>	<b>9</b>
<b>2.1</b>	<b>Polarization.....</b>	<b>9</b>
2.1.1	Linear polarized wave .....	9
2.1.2	Circular polarized wave .....	11
2.1.3	Polarization Choice for MAV.....	12
<b>2.2</b>	<b>Methods for Polarity-free .....</b>	<b>13</b>
2.2.1	UMA Method .....	13
2.2.2	SPFA Method .....	14
<b>Chapter 3</b>	<b>Theories of Rectenna elements.....</b>	<b>15</b>
<b>3.1</b>	<b>Theory of Rectenna Design .....</b>	<b>15</b>
<b>3.2</b>	<b>Theory of Antenna Design.....</b>	<b>17</b>
3.2.1	Size Designing of MSA .....	17
3.2.2	Impedance Matching Method between MSA element and Feeding System.....	17
3.2.3	Interior Electromagnetic Field of Rectangular MSA .....	19
<b>3.3</b>	<b>Theory of Rectifier Circuit Design .....</b>	<b>23</b>
3.3.1	Rectifier Circuit Model in Lumped Parameter System.....	24
3.3.2	Matching of Input Impedance .....	26
3.3.3	Design of Stub.....	27
3.3.4	Output load-line Characteristics.....	28
3.3.5	Rectifier Circuit Model in Distributed Parameter System .....	30
<b>Chapter 4</b>	<b>Experimental Apparatus .....</b>	<b>31</b>
<b>4.1</b>	<b>Power Transmission System.....</b>	<b>31</b>
4.1.1	Oscillator.....	33
4.1.2	Power divider .....	34

4.1.3	6-bit digital phase shifter.....	35
4.1.4	Driver amplifier .....	37
4.1.5	Power amplifier.....	38
4.1.6	Booster amplifier .....	40
4.1.7	Horn antenna.....	41
<b>4.2</b>	<b>Power Receiving System / Measurement Apparatus.....</b>	<b>42</b>
4.2.1	Patch antenna .....	42
4.2.2	Rectifier.....	43
4.2.3	Open/Load switching unit.....	44
4.2.4	Oscilloscope.....	46
<b>4.3</b>	<b>Experimental Setup and Others .....</b>	<b>47</b>
4.3.1	Mounting structure.....	47
4.3.2	Substrate.....	48
4.3.3	Electrical Motor for Demonstration.....	49
<b>Chapter 5</b>	<b>Measurement Results and Discussions.....</b>	<b>50</b>
<b>5.1</b>	<b>Polarity-Free Antenna .....</b>	<b>50</b>
5.1.1	Polarity-Free Antenna Designing.....	50
5.1.2	Effects of Antenna Patterns.....	51
5.1.3	Effects of Chamfering Ratio .....	52
5.1.4	Assumption and Simulation of Current Distributions on MSA .....	53
5.1.5	Comparison with Unit of Multiple Dipole Antennas .....	55
<b>5.2</b>	<b>Optimization of Rectifier Circuit.....</b>	<b>56</b>
5.2.1	Type of Schotkky Barrier Diode: $D$ .....	58
5.2.2	Capacitance of Chip Condenser: $C_0$ .....	59
5.2.3	Input Width: $W$ .....	60
5.2.4	Input Length: $l_{in}$ .....	61
5.2.5	Width between Diode and Ground: $W_g$ .....	63
5.2.6	Length between Diode and Ground: $l_g$ .....	64
5.2.7	Stub Length after Diode: $l_s$ .....	65
5.2.8	Output Transmission Line (OTL) Length: $l_{tl}$ .....	66
5.2.9	Low Pass Filter (LPF) Shape: $W_C, l_C$ .....	67
5.2.10	Output Length: $l_{out}$ .....	68
5.2.11	Redesign of Rectifier Circuit .....	69
<b>5.3</b>	<b>Rectenna Demonstration .....</b>	<b>71</b>
5.3.1	Combining Antenna with Rectifier .....	71
5.3.2	Parallel Connection of Rectenna.....	72

5.3.3	Demonstration.....	74
<b>Chapter 6</b>	<b>Conclusions.....</b>	<b>75</b>
<b>6.1</b>	<b>Conclusions.....</b>	<b>75</b>
<b>6.2</b>	<b>Future Perspectives and Issues .....</b>	<b>76</b>
<b>References.....</b>		<b>77</b>
<b>Acknowledgements .....</b>		<b>80</b>

# Table of Figures

Figure 1.1 Schematic of Tracking Problem.....	2
Figure 1.2 Angle Definitions for Aerial Vehicles.....	2
Figure 1.3 Schematic of Target Tracking System .....	3
Figure 1.4 Block Diagram of Tracking System .....	4
Figure 1.5 Schematic of Beam Steering by Phased Array Antennas.....	4
Figure 1.6 $E_y$ Distribution at $h=1\text{m}$ .....	5
Figure 1.7 Computed Main-lobe Fractional Energy and Beam Divergence Angle.....	5
Figure 1.8 Effect of Pitch Angle at $(x,y,z)=(0,0,62)$ [cm] .....	6
Figure 1.9 Examples of Polarization-Plane Characteristic.....	7
Figure 2.1 Schematic of Planar wave (TEM) Propagation .....	10
Figure 2.2 Schematic of Rotating Polarization Plane .....	11
Figure 2.3 Pattern of Unit of Multiple Dipole Antenna .....	13
Figure 2.4 Pattern of Patch Antenna for Circular Polarized Wave.....	14
Figure 3.1 Schematic of Rectenna .....	16
Figure 3.2 RF-DC Conversion Efficiency of Rectenna .....	16
Figure 3.3 Feeding Methods of MSA Element .....	18
Figure 3.4 Rectanglar MSA and its Coordinate System.....	19
Figure 3.5 Schematic of Electromagnetic Distribution of $TM_{100}$ wave .....	22
Figure 3.6 Simple Schematic of Rectifier Circuit with Input and Output Filters .....	23
Figure 3.7 Schematic of Rectifier Circuit with Lumped-element Input and Output Filters.....	24
Figure 3.8 Schematic of Rectifier Circuit with a Transmission Line as Output Filter.....	24
Figure 3.9 Rectifier Circuit Pattern.....	25
Figure 3.10 Schematic of Rectifier Circuit for Experiment.....	25
Figure 3.11 Structure of Micro-Strip Line .....	26
Figure 3.12 Pattern and Equivalent Circuit of Micro-Strip Stub .....	27
Figure 3.13 Relationship between DC equivalent circuit and load-line.....	28
Figure 3.14 V-I Characteristic of Diode.....	29
Figure 3.15 Equivalent Circuit of Diode.....	30
Figure 3.16 Detailed Schematic of Rectifier Circuit for Experiment.....	30
Figure 4.1 Schematic of Transmitting Array antenna System.....	31
Figure 4.2 Picture of Transmitting System (1: Power Amplifiers, 2: Driver Amplifiers, 3: Phase Shifters, 4: Booster Amplifier, 5: Oscillator, 6: 8 Power Divider, 7: Power Source).....	32
Figure 4.3 Arrangement of five antenna elements of the array.....	32

---

Figure 4.4 Picture of Oscillator.....	33
Figure 4.5 Picture of Power Divider .....	34
Figure 4.6 Picture of Phase Shifter .....	35
Figure 4.7 Mechanism of phase shifting.....	35
Figure 4.8 Picture of Driver Amplifier.....	37
Figure 4.9 Picture of Power Amplifier.....	38
Figure 4.10 Characteristic of Power Amplifier .....	39
Figure 4.11 Relationship of Temperature and Output Voltage of Power Amplifier .....	39
Figure 4.12 Picture of Booster Amplifier.....	40
Figure 4.13 Picture of Horn Antenna .....	41
Figure 4.14 Size of Horn antenna .....	41
Figure 4.15 Schematic of Power Receiving System .....	42
Figure 4.16 Picture of Patch Antenna .....	42
Figure 4.17 Picture of Rectifier.....	43
Figure 4.18 Characteristic of Rectifier.....	43
Figure 4.19 Picture of Open/Load Switching Unit .....	44
Figure 4.20 Schematics of Load/Open Switching Unit.....	45
Figure 4.21 Pictures of Oscilloscopes.....	46
Figure 4.22 Picture of Mounting Structure .....	47
Figure 4.23 Picture of Electrical Motor .....	49
Figure 5.1 Antenna Patterns.....	50
Figure 5.2 Picture of Handmade MSA Patterns.....	50
Figure 5.3 Angle Dependency Characteristics (Antenna Patterns).....	51
Figure 5.4 Angle Dependency Characteristics (Chamfering Ratios).....	52
Figure 5.5 Current Distributions of MSAs (a: square, b: ACPW, c: Leaf).....	54
Figure 5.6 Comparison Leaf MSA with UMDA.....	55
Figure 5.7 Schematic of Rectifier Circuit Pattern Parameters .....	57
Figure 5.8 Load Characteristic related to SBD .....	58
Figure 5.9 Load Characteristic related to Capacitance .....	59
Figure 5.10 Load Characteristic related to Input Width.....	60
Figure 5.11 Load Characteristic related to Input Length .....	62
Figure 5.12 Schematic of 2 End Terminals of Distributed Parameter Line .....	62
Figure 5.13 Load Characteristic related to D-G Width .....	63
Figure 5.14 Load Characteristic related to D-G Length.....	64
Figure 5.15 Relationship between Stub Length and Output Voltage .....	65
Figure 5.16 Load Characteristic related to OTL Length .....	66

---

Figure 5.17 Load Characteristic related to LPF shape .....	67
Figure 5.18 Load Characteristic related to Output Length.....	68
Figure 5.19 Load Characteristic before and after Redesigning.....	70
Figure 5.20 Picture of Rectenna Array (Rectifier Face).....	73
Figure 5.21 Picture of Rectenna Array (Antenna Face).....	73
Figure 5.22 Coordinate System of Horn Antenna.....	74



## Table of Tables

Table 4.1 Specifications of Transmitting Array Antenna System .....	32
Table 4.2 Specifications of Oscillator .....	33
Table 4.3 Specification of Phase Shifter No.2 (Lot No. 40915953) .....	36
Table 4.4 Specification of Phase Shifter No.3 (Lot No. 40405819-2) .....	36
Table 4.5 Specification of Phase Shifter No.4 (Lot No. 40405819-1) .....	36
Table 4.6 Specification of Phase Shifter No.5 (Lot No. 50218076) .....	37
Table 4.7 Specification of Driver Amplifier .....	37
Table 4.8 Specification of Power Amplifiers .....	39
Table 4.9 Specification of Booster Amplifier .....	40
Table 4.10 Specifications of Oscilloscopes.....	46
Table 4.11 Specification of Substratum .....	48
Table 4.12 Specification of Electrical Motor .....	49
Table 5.1 Specifications of Best Polarity-Free MSA .....	52
Table 5.2 Parameters for Standard Rectifier Circuit Pattern .....	57
Table 5.3 Parameters of Redesigned Rectifier Circuit Pattern.....	69
Table 5.4 Parameters for Rectenna Array .....	71

# Chapter 1 Introduction

This chapter shows the background and the problems of this thesis.

## 1.1 Power Supply System for Innovative Aerial Robot Project

At the University of Tokyo, a project for Micro Aerial Vehicles (MAV) and Unmanned Aerial Vehicles (UAV), “Innovative Aerial Robot Project (IARP)”, was being carried out as part of the 21st century Centers of Excellence (COE) program, “Mechanical Systems Innovation”. The objective of IARP was achieving the sophisticated aerial vehicles executing the target missions; flying to its destinations autonomously, and surveying with a bird’s-eye view continually for a long time. In this project, we took charge of the power supply system for MAV. We considered three methods as the system: taking-off and landing, wired and wireless.

In the taking-off and landing method, we install the power sources, such as batteries and fuel, on MAV and resupply it with taking-off and landing. However, this method has a limited carrying capacity of it. Moreover, although we have to keep its runaway space during the mission because MAV needs to take-off and land at short intervals, it is difficult in practice. From these reasons, this method is unsuitable for the project.

In the wired method, MAV was connected the power supplier on the ground by wire directly. Thus it is unnecessary to take-off and land for resupplying and to keep the runaway space continuously except for the first taking-off and the last landing. However, we would use the method only for the fixed-point observations over the power supplier because of the limited activity of MAV by the cable length. Therefore, this method is also unsuitable for the project.

In the wireless method, for supplying power from the ground, we use the electromagnetic waves, such as light and microwaves, instead of the cable. Microwave is less affected by the weathers, but the focusing property of it is weaker than of light. Moreover, since we can track the target actively not with moving the transmitting antennas but with using microwave and controlling its phase, the method is suitable to supply power for high-speed aerial vehicles. Although MAV can fly continuously without installing the power source by creating the power transmitting system along its flight path, it is more practical that MAV equipped with batteries circles over the system and resupplies power when it got low on power.

In the project, our objectives are the developments of the power transmission system with microwave of 5.8GHz for MAV. In this thesis, especially, I studied and developed the receiving rectenna capable of the stable power supply for MAV circling over the transmission system.

## 1.2 Problems with MAV Circling

There are three main problems with MAV circling: target tracking, effects of the pitch and the roll angles and of the yaw angle. Figure 1.1 shows the schematic of the target tracking problem and Figure 1.2 shows the angle definitions for aerial vehicles.

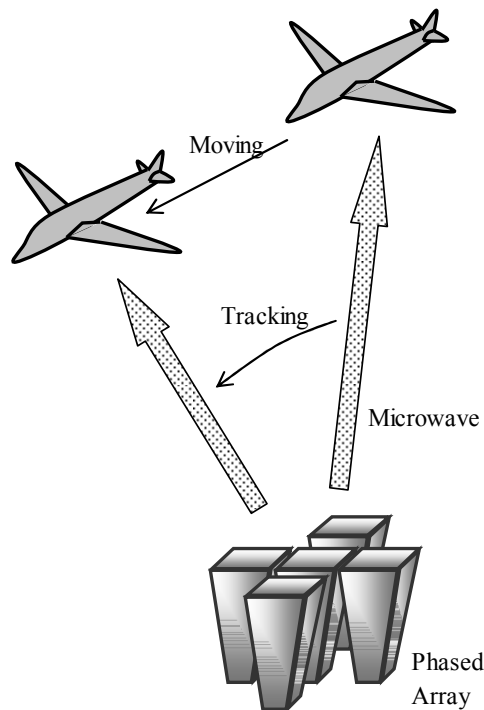


Figure 1.1 Schematic of Tracking Problem

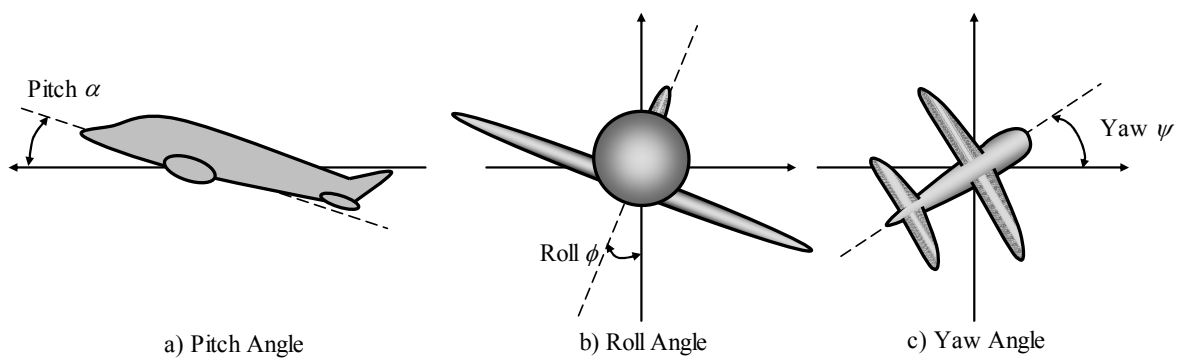


Figure 1.2 Angle Definitions for Aerial Vehicles

### 1.2.1 Target Tracking

The target position changes continuously because the MAV is moving, and then we required the target tracking system.<sup>1,2</sup> It consisted of the three parts: tracking system, phase controlling and power transmitting. Figure 1.3 shows its schematic.

First, MAV transmits the pilot signal to the tracking system. Figure 1.4 shows the block diagram of the tracking system. The incident pilot signal is received by two or three antennas, and the microwave elements are divided and combined, and then rectified and measured as the output voltages. From the measured voltages, we can find the incident angles of the pilot signal, or the target position. With this target position, the shifting phases for each transmitting antenna lines are calculated and the instructions of the phase shift are sent to the phase shifters. As seen in Figure 1.5, the microwaves with phase controlled reinforce each other to a beam steering angle of  $\theta_{str}$  expressed as:

$$d \sin \theta_{str} = \frac{\lambda \delta}{2\pi} \quad (1.1)$$

where  $\lambda$  is the wavelength and  $\delta$  is the phase difference.

Figure 1.6 shows the computed and measure beam profiles. Measured main-lobe fractional energy and main-lobe beam divergence angle are well agreed with the calculated ones. Figure 1.7 shows the computed properties as a function of  $\theta_{str}$ . The beam divergence was constant at about nine degrees, which corresponds to the beam quality of  $M^2=1.6$ .

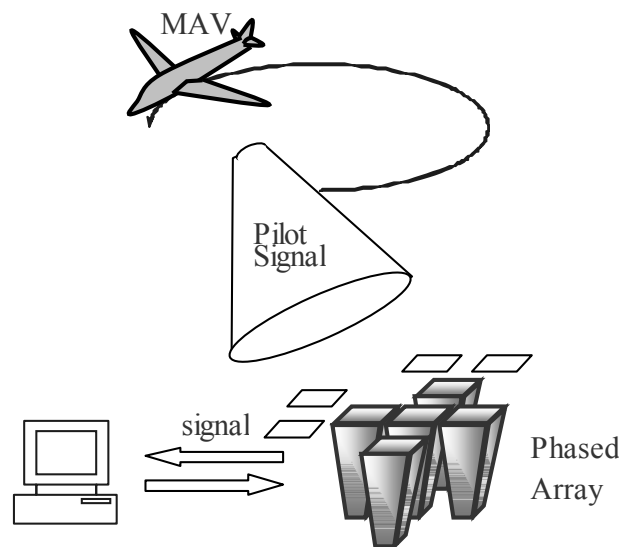


Figure 1.3 Schematic of Target Tracking System

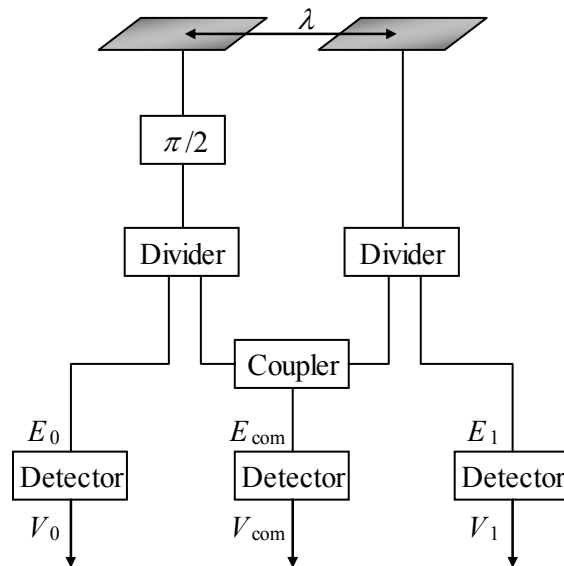


Figure 1.4 Block Diagram of Tracking System

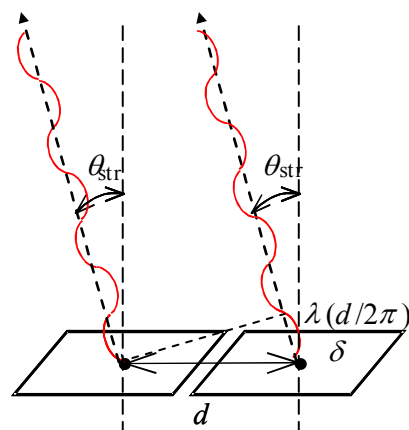
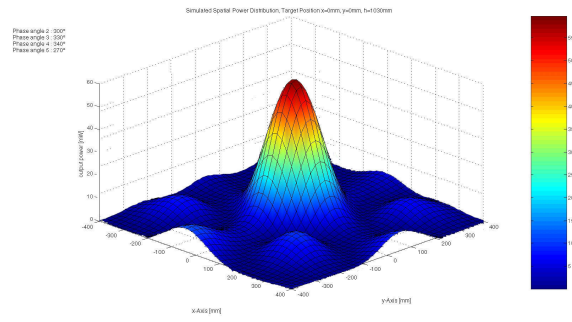
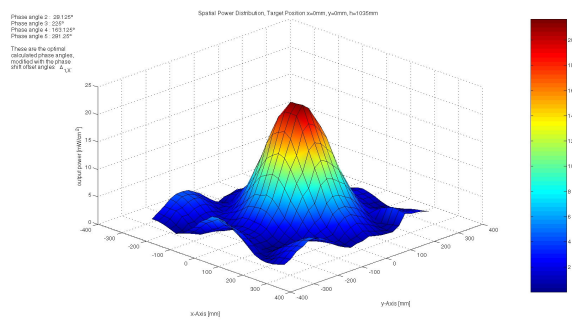


Figure 1.5 Schematic of Beam Steering by Phased Array Antennas



a) Computed



b) Measured

Figure 1.6  $E_y$  Distribution at  $h=1m$

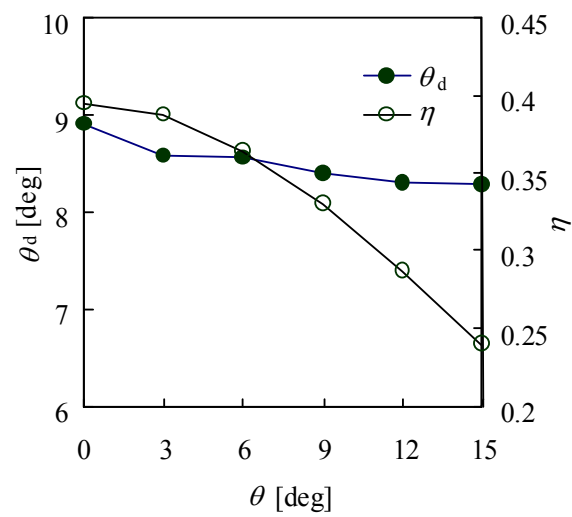


Figure 1.7 Computed Main-lobe Fractional Energy and Beam Divergence Angle

### 1.2.2 Effects of Pitch and Roll Angles

Since both the pitch angle  $\alpha$  and the roll angles  $\phi$  are the inclination angles of the plane parallel to the horizon plane, we cannot obtain the cosine element of the incident power  $P_{in}$  expressed as:

$$P_{\alpha} = P_{in} \cos \alpha \quad (1.2)$$

$$P_{\theta} = P_{in} \cos \theta \quad (1.3)$$

where  $P_{\alpha}$  and  $P_{\theta}$  are the obtained powers with the incident angle of  $\alpha$  and  $\theta$ .

Figure 1.8 show the measurement result with changing pitch angle  $\alpha$  in the past research.<sup>1</sup> As seen in the graph, the report concluded that they are represented approximately as:

$$P_{\alpha} = P_{in} \cos^2 \alpha \quad (1.4)$$

$$P_{\theta} = P_{in} \cos^2 \theta \quad (1.5)$$

Although the effects would be ignored because the angle differences of  $\alpha$  and  $\phi$  of Flying MAV are enough small, but we need measures to prevent the angle generations; keeping the antenna plane parallel to the horizon plane by hanging or by changing the install angle mechanically or so.

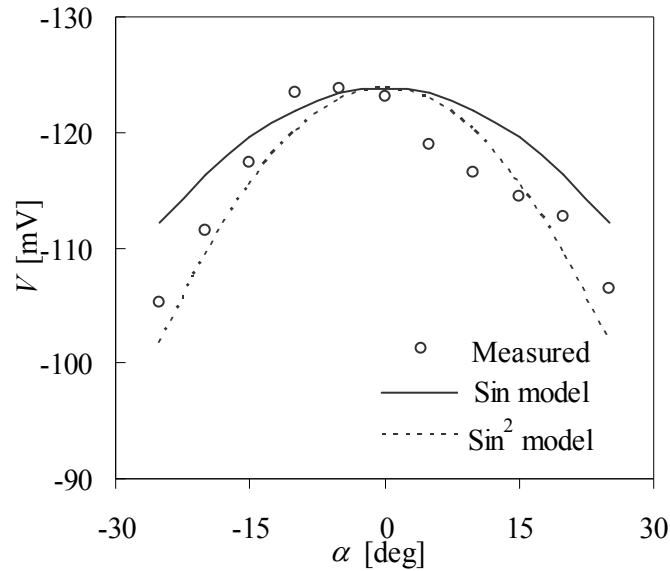
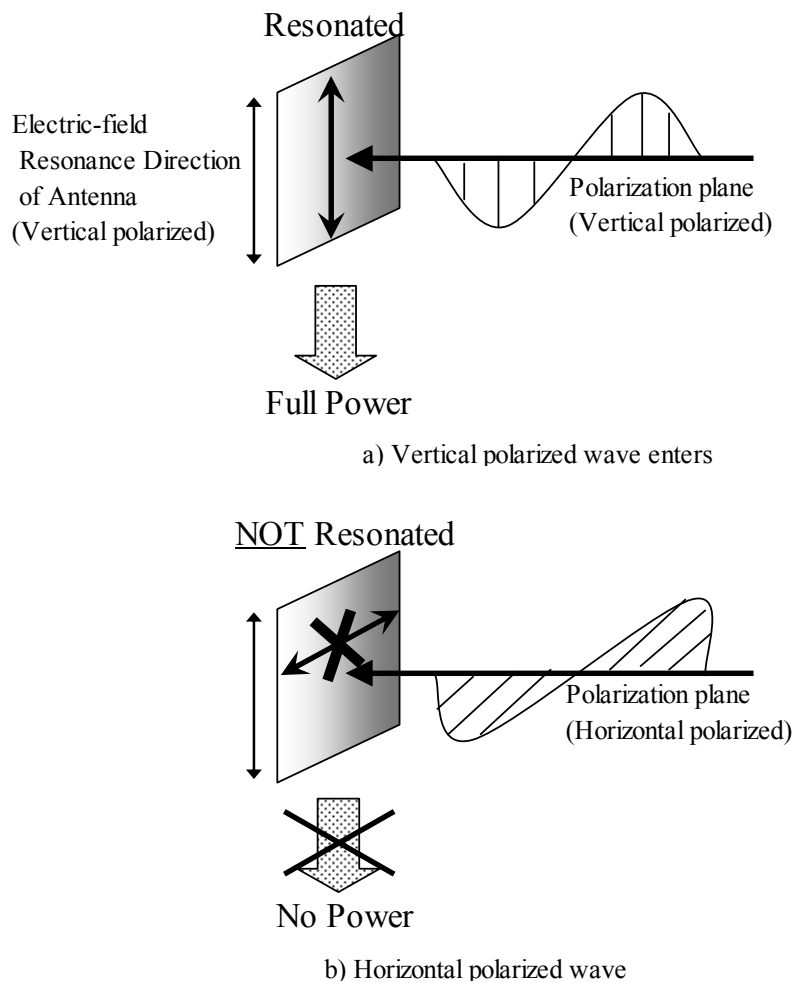


Figure 1.8 Effect of Pitch Angle at  $(x,y,z)=(0,0,62)$  [cm]

### 1.2.3 Effects of Yaw Angle

For MAV flying with microwave power supply system, I regarded the effects of the yaw angle as the most important problems. The problem is associated with the polarization-plane characteristic. Every electromagnetic wave has a polarization, and every antenna also does. With the linear polarization wave, when the polarization-planes of the incident electromagnetic wave and antenna's resonance direction are synchronized, we are able to obtain full the transmitting power. However, when they are not synchronized, we will get less power, or no power.<sup>3</sup> Figure 1.9 show the examples. First, the electric-field resonance direction of the receiving antenna is vertical. When the incident wave is vertically polarized, we will able to obtain full the incident power because of the electric-field resonance. Moreover, when it is horizontally polarized, we will able to obtain no power because of no resonance. Therefore, the problem of yaw angle, or the polarization-plane characteristic is fatal for the project. I show the more details in the chapter 2.



**Figure 1.9 Examples of Polarization-Plane Characteristic**



### **1.3 Other Applications with Power Transmitting System**

For IARP, we developed the power transmitting system and the power receiving system with microwave for MAV, and we can apply the technology to wider areas. One of the advantages of this system is supplying power continuously within the microwave receivable area, without installing batteries or connecting to the power supplier by wire. Therefore, the technology will be suitable for such robot as searching for and rescuing victims trapped under heavy debris by disasters and as scanning and discovering and repairing cracks and other troubles of pipes with moving in it.

Moreover, the polarity-free rectenna, developed in my study, especially achieved the stable power supply independent from the incident wave polarization in its small size. I consider that we can apply this technology to micro robots moving independently without remote control and mobile devices running not with batteries but with the receiving power in spaces filled with microwave.

## Chapter 2

# Theory of Polarity-Free Antenna

This chapter describes about the theory of the wave polarization and the methods of making the receiving system polarity-free.

### 2.1 Polarization

There are two polarized waves; linear polarized wave and circular polarized wave. I explain the polarization theories and the reasons why the polarity-free antennas are needed below.

#### 2.1.1 Linear polarized wave

Electromagnetic wave, including microwave, has a polarization. When an electromagnetic wave propagates through an uniform medium, the Maxwell equations are expressed with a charge density  $\rho=0$  as:<sup>4,5</sup>

$$\left. \begin{aligned} \nabla \times \mathbf{E} &= -\mu \frac{\partial \mathbf{H}}{\partial t} \\ \nabla \times \mathbf{H} &= \sigma \mathbf{E} + \varepsilon \frac{\partial \mathbf{E}}{\partial t} \\ \nabla \cdot \mathbf{E} &= 0 \\ \nabla \cdot \mathbf{H} &= 0 \end{aligned} \right\} \quad (2.1)$$

where  $\varepsilon$  is a dielectric constant and  $\mu$  is a conductivity of the medium. Generally, an electromagnetic wave varies at a constant frequency as sine curve, the electric field  $\mathbf{E}$  and the magnetic field  $\mathbf{H}$  are expressed as:

$$\mathbf{E} = \mathbf{E}_0 e^{i\omega t} \quad (2.2)$$

$$\mathbf{H} = \mathbf{H}_0 e^{i\omega t} \quad (2.3)$$

where  $\omega$  is an angular frequency. Since they include phase terms, these  $\mathbf{E}$ ,  $\mathbf{E}_0$ ,  $\mathbf{H}$ ,  $\mathbf{H}_0$  are complex variables and the absolute values of  $\mathbf{E}_0$ ,  $\mathbf{H}_0$  are the amplitude of the electric field and that of the magnetic field. The real waves are expressed by their real parts.

Moreover, let the partial differentiation about time  $t$   $\partial/\partial t = j\omega$  and divide the electrical field and the magnetic field to  $x$ ,  $y$  and  $z$  element, then the equation (2.1) is converted as:

$$\left. \begin{aligned}
 \frac{\partial E_z}{\partial y} - \frac{\partial E_y}{\partial z} &= -j\omega\mu H_x \\
 \frac{\partial E_x}{\partial z} - \frac{\partial E_z}{\partial x} &= -j\omega\mu H_y \\
 \frac{\partial E_y}{\partial x} - \frac{\partial E_x}{\partial y} &= -j\omega\mu H_z \\
 \frac{\partial H_z}{\partial y} - \frac{\partial H_y}{\partial z} &= (\sigma + j\omega\varepsilon)E_x \\
 \frac{\partial H_x}{\partial z} - \frac{\partial H_z}{\partial x} &= (\sigma + j\omega\varepsilon)E_y \\
 \frac{\partial H_y}{\partial x} - \frac{\partial H_x}{\partial y} &= (\sigma + j\omega\varepsilon)E_z
 \end{aligned} \right\} \quad (2.4)$$

When an electromagnetic wave propagates as a planar wave, there is no change of the electric field and the magnetic field in the  $x$ - $y$  plane at right angles to the propagating direction ( $z$  axis). Or the solutions differentiating these fields with respect to  $x$  and  $y$  are 0. Under this condition, the  $z$  axial component of the electromagnetic field varying temporally is expressed as:

$$E_z = H_z = 0 \quad (2.5)$$

Figure 2.1 shows the electromagnetic wave called “transverse electro magnetic (TEM) wave” or “linear polarized wave;” the temporally homogeneous electromagnetic wave without the component in the propagation direction of the electric field and the magnetic field. Additionally the plane formed by the direction of the electric field and the wave propagating direction is called the “polarization plane.”

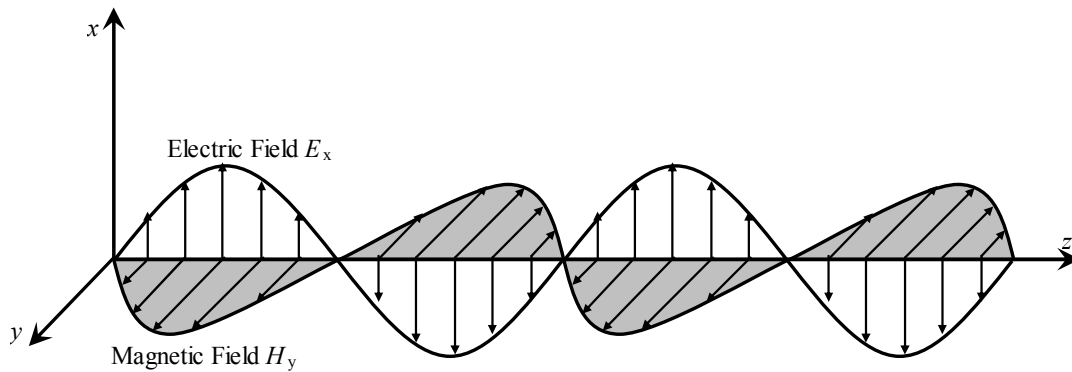


**Figure 2.1 Schematic of Planar wave (TEM) Propagation**

As a result, the equation (2.4) is figured as:

[x-direction polarization]

$$\begin{aligned}\frac{\partial E_x}{\partial z} &= -j\omega\mu H_y \\ \frac{\partial H_y}{\partial z} &= -(\sigma + j\omega\varepsilon)E_x\end{aligned}\quad (2.6)$$

[y-direction polarization]

$$\begin{aligned}\frac{\partial E_y}{\partial z} &= -j\omega\mu H_x \\ \frac{\partial H_x}{\partial z} &= -(\sigma + j\omega\varepsilon)E_y\end{aligned}\quad (2.7)$$

The  $x$ -direction polarization has only an  $x$  component of the electric field and a  $y$  component of the magnetic field as Figure 2.1, and the  $y$ -direction polarization is the equivalent of the  $x$ -direction one rotated by 90 degrees around the propagation direction. Furthermore, they can exist independently of each other. With the linear polarized wave, we can obtain power only with the antennas of the same polarization as the incident wave: the set of horizontal antennas and horizontal wave, or of vertical antennas and vertical wave.

### 2.1.2 Circular polarized wave

Linear polarized waves are able to generate only artificially, and the polarization plane of natural electromagnetic waves are temporally rotating. Figure 2.2 shows its schematic. It is called “circular polarized wave.” We can generate circular polarized waves by combining the linear polarized waves.

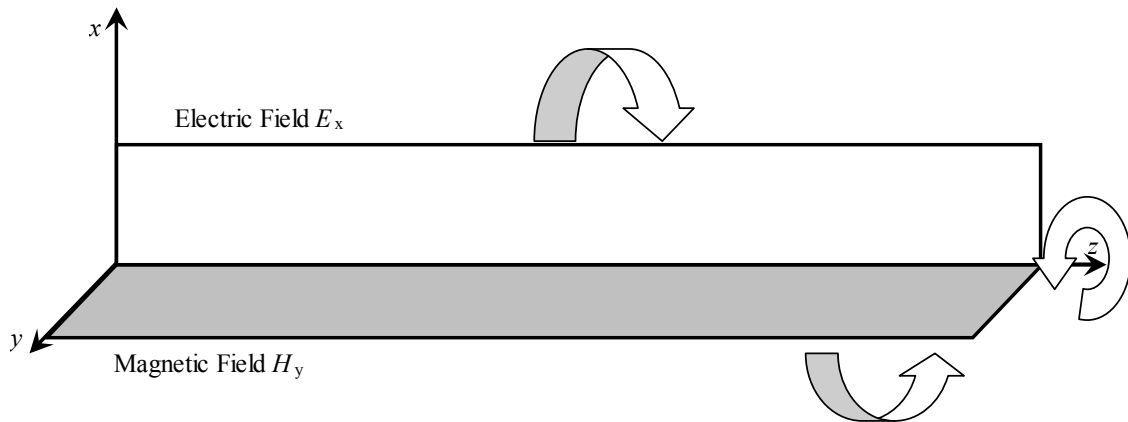


Figure 2.2 Schematic of Rotating Polarization Plane

When there are two linear polarized waves, the electric field component of the  $x$ -direction polarized wave is expressed as:

$$E_x = a \cos(\omega t - \beta z) \quad (2.8)$$

where  $\beta$  is a phase constant, and that of the  $y$ -direction polarized wave with the phase delaying by  $\delta$  is also expressed as:

$$E_y = b \cos(\omega t - \beta z - \delta) \quad (2.9)$$

When two polarized waves with different phases exist, the circular polarized wave is generated with combining them. (When there is no phase difference, or  $\delta=0$ , the combined wave is just a linear polarized wave at an angle with the  $x$ -axis.)

Under the special condition where  $\delta=\pi/2$ ,  $a=b$ ,  $E_x$  and  $E_y$  are represented as:

$$\left. \begin{aligned} E_x &= a \cos(\omega t - \beta z) \\ E_y &= a \cos(\omega t - \beta z - \pi/2) = a \sin(\omega t - \beta z) \end{aligned} \right\} \quad (2.10)$$

and then:

$$E_x^2 + E_y^2 = a^2 \quad (2.11)$$

From this, the combined electric field plane is rotating around any  $z$  position within its radius  $a$ . In turn, this wave is propagating to the  $z$  direction at the phase velocity  $v_p$  with rotating around the  $z$ -axis at the angular rate  $\omega$ . This wave called ‘‘circular polarized wave.’’ Under the general condition where not both  $\delta=\pi/2$  and  $a=b$ , the field locus is the ellipse and the wave called ‘‘elliptical polarized wave.’’

### 2.1.3 Polarization Choice for MAV

In this thesis, since the objective was the power transmission, not signal transmission, I needed the high-efficient and simple system. The circular polarized wave can ignore the characteristic of the polarization plane. However, it is unsuitable for the power transmission because of its lower transmitting efficiency by reflections with transmitting and receiving than the linear one. The linear one can achieve high efficiency and simple control system, then as with many researches, I adopted it for the power transmitting system. Furthermore, since the MAV will move with random yaw angle in spite of the fixed polarization plane by the linear polarized transmitting wave, we need to make the receiving device polarity-free.

## 2.2 Methods for Polarity-free

Generally, there are two methods to make receiving antennas polarity-free: one method is a unit of multiple antennas (UMA) with different polarization angles, and another is a self polarity-free antenna (SPFA).

### 2.2.1 UMA Method

The UMA method is making an antenna-unit combining some normal polarized antennas, such as dipole antennas and patch antennas, and arranging them in predetermined design. It enables to supply stable power as the unit by antenna elements covering for each other's weak angles. Figure 2.3 shows the unit of multiple dipole antennas (UMDA). One of the advantages is the calculation simplicity of the polarization-angle dependency and the power conversion efficiency because the UMA consists of the existing antennas. Furthermore, a flexible UMDA sheet has been developed. However, the disadvantages are the low conversion efficiency and the large size because it needs some antennas for achieving polarity-free and the utilizable power is the average obtained from them. Moreover, some rectifier circuits are also needed.

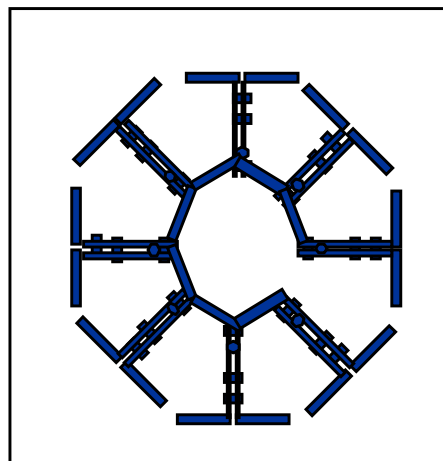
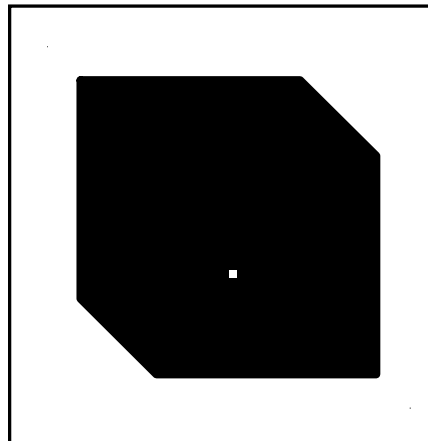


Figure 2.3 Pattern of Unit of Multiple Dipole Antenna

### 2.2.2 SPFA Method

The SPFA method is making an antenna itself polarity-free without any excessive antenna area. The advantage is the smallness of its minimum unit area; about one ninth the size of the UMDA. Moreover, since it requires only one rectifier circuit in a unit, its structure is very simple. These advantages are suitable for the MAV-installed system. However, the disadvantage is the design; the completely SPFA has not been reported. Therefore, I surveyed the SPFA design based on patch antenna for circular polarized wave (ACPW) in Figure 2.4.



**Figure 2.4** Pattern of Patch Antenna for Circular Polarized Wave

## Chapter 3

# Theories of Rectenna elements

This chapter shows the theories of the rectenna elements including antenna elements and rectifier circuit elements.

### 3.1 Theory of Rectenna Design

“Rectenna” is a device receiving the transmitted microwave power as radio frequency (RF) and converting alternating current (AC) to direct current (DC) by rectifying. It is the coined term for “RECTifier” and “antENNA”. Figure 3.1 shows its schematic. It normally consists of a receiving antenna, an input filter, a rectifier and a output filter for smoothing power. Since the receivable power with a rectenna is not enough large to operate systems, we use as a array of some rectennas arranged and connected in series and in parallel each other.

One of the determining factors of the power conversion efficiency of a rectenna is the characteristic of the important element of a rectifier, or a diode.<sup>6</sup> Figure 3.2 shows the RF-DC conversion efficiency characteristic of a rectenna. When the input power  $P_{in}$  decrease, the conversion efficiency  $\eta$  will become reduced. It is because the voltage between the both ends of a diode  $V_d$  will become smaller than the diode forwarding voltage  $V_f$ , and then the rectifying feature of the diode will not work (the  $V_f$  effect). Although the conversion efficiency increase as  $P_{in}$  becomes larger, when  $V_d$  surpass the diode breakdown voltage  $V_R$ ,  $\eta$  will also become reduced. It is because the reverse current starts to flow (the  $V_R$  effect). Moreover,  $\eta$  will also become reduced because the high order radio-frequency re-radiation generated with rectifying (the higher order harmonics effect).

Furthermore, the load resistance connected to the rectenna output has the optimal values; it is the value in matching the output impedances of the rectenna with the load and also depends on  $P_{in}$ . Although there is no reflected wave with connecting the optimal load, there is reflected waves and  $\eta$  decreased without it. As a result, the diode maximum efficiency curve has a peak value depending on the input power  $P_{in}$  and the load resistance  $R_L$ .



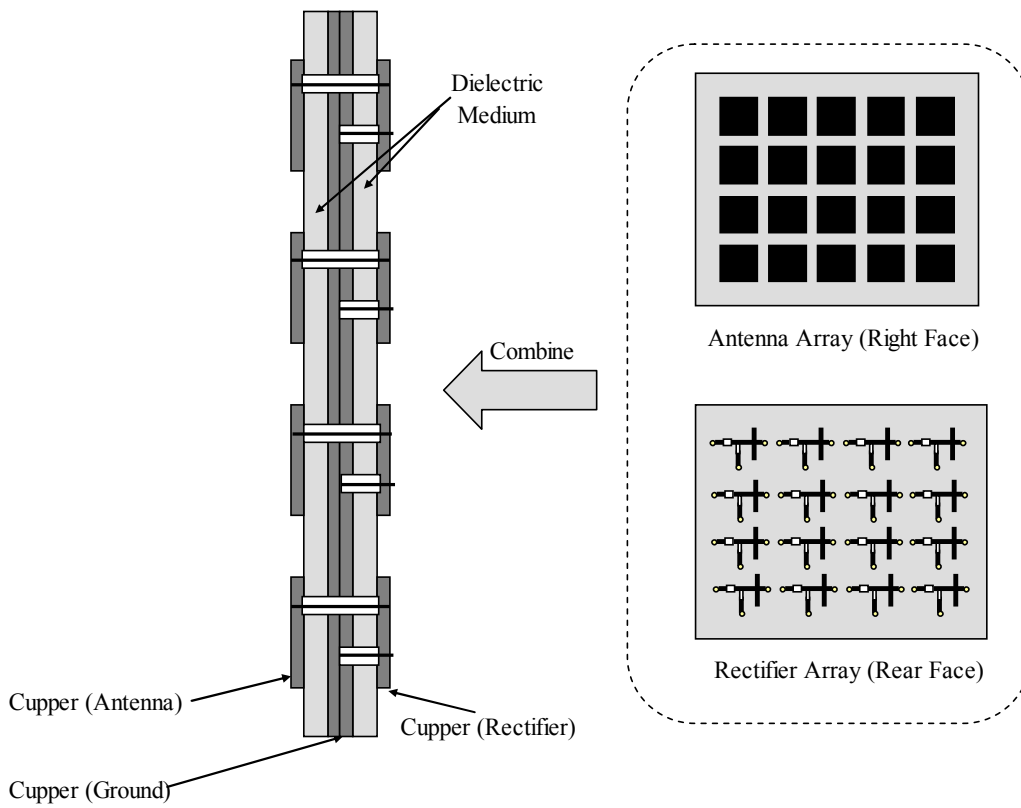


Figure 3.1 Schematic of Rectenna

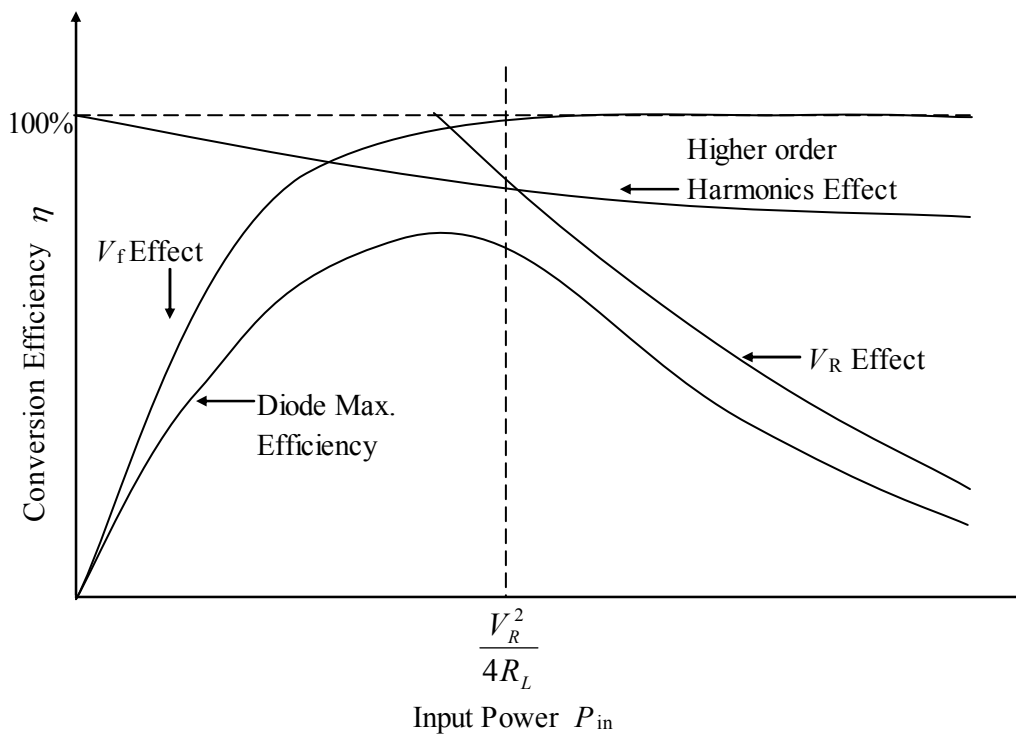


Figure 3.2 RF-DC Conversion Efficiency of Rectenna

## 3.2 Theory of Antenna Design

There are many kinds of Antenna; horn antennas, monopole antenna, dipole antennas, slot antennas, *etc.*<sup>7-9</sup> In this thesis, we adopted the plane patch antennas because of the simplicity of structure, the miniaturization in the size and the lightness.

The typical examples of the plane antennas are MSA (Micro Strip Antenna) elements. They function as the microwave radiators composed of the planar circuit resonance elements with the circular or quadrangular open boundary on the printed circuit boards (PCBs). Generally the substrate for the MSA require low dielectric constant ( $\epsilon_r = 1.2 \sim 5.0$ ) and low dielectric loss ( $\tan \delta = 10^{-3} \sim 10^{-4}$ ), such as the teflon-fiberglass substrate. In request for weight saving of wider band width (low  $Q$  value), the paper-honeycomb substrate are used.

The size of the MSA elements is normally the half wavelength or less. The main mode is used as a specimen excitation mode, and the MSA radiation pattern of the main mode shows the unidirectionality with the maximum value in the front direction ( $z$ -axis) of the antenna pattern of both the circular and quadrangular MSA. Thus, MSA enables to achieve the unidirectional pattern without additional reflectors and to compose the thin and compact antenna simply.

### 3.2.1 Size Designing of MSA

The size of antennas depends on the target microwave wavelength. Generally the half wavelength resonance method is used, and its resonance direction length is  $\lambda_g/2$ . The  $\lambda_g$  is the wavelength of the microwave passing through a medium and is approximately expressed by:<sup>10,11</sup>

$$\lambda_g = \frac{\lambda_0}{\sqrt{\epsilon_r}} \quad (3.1)$$

where  $\lambda_0$  is the free-space wavelength and  $\epsilon_r$  is the dielectric constant of the medium. In this thesis, the size of square MSA for 5.8GHz was about 1.22cm on a side, 1.484cm<sup>2</sup> with the glass-epoxy substrate FR-4 ( $\epsilon_r=4.7$ ). I explain the more details in the section 3.2.3.

### 3.2.2 Impedance Matching Method between MSA element and Feeding System

Figure 3.3 shows the typical feeding methods of the MSA. The input impedance  $Z_{in}$  of the MSA excited in the main mode depends on the predetermined feeding point  $\rho_0$ .<sup>12</sup>  $Z_{in}$  at the resonance point and around the near frequency domain vary from 0 (center) to several hundred ohms (open boundary) by  $\rho_0$ . Thus, with feeding at the edge (open boundary) of the MSA elements, the resonance  $Z_{in}$  exhibits a high impedance characteristic about 300~500 $\Omega$ . Consequently, we need for it to match up with the feeding system about 50 $\Omega$  of the characteristic impedance. In the backside-coaxial feeding method, we can match up the impedances by offsetting the position  $\rho_0$  of the feeding point F. Generally, the offset ratio is about 30%; ( $\rho_0/a$ )=0.3 in the circular MSA,

( $\rho_0/(a/2)=0.3$ ) in the quadrangular MSA. In the coplanar feeding method, we can also match up the impedance of the antenna with one of the main feeding line  $F_m$  by the  $\lambda_g/4$  impedance transformer  $T_f$ . In the electromagnetic coupling feeding method, it is adopted to set the insert length  $l_0$  to the specimen excitation slot of the feeding strip line at about  $\lambda_g/4$ , and to control the values of the specimen excitation slot width  $w$ , its slot length  $l_s$  and the offset length  $\rho_0$ . In this thesis, we adopted the backside-coaxial feeding method and 0.3 of  $\rho_0$  because of the simplicity of its fabrication and the connectivity with the rectifier circuits.

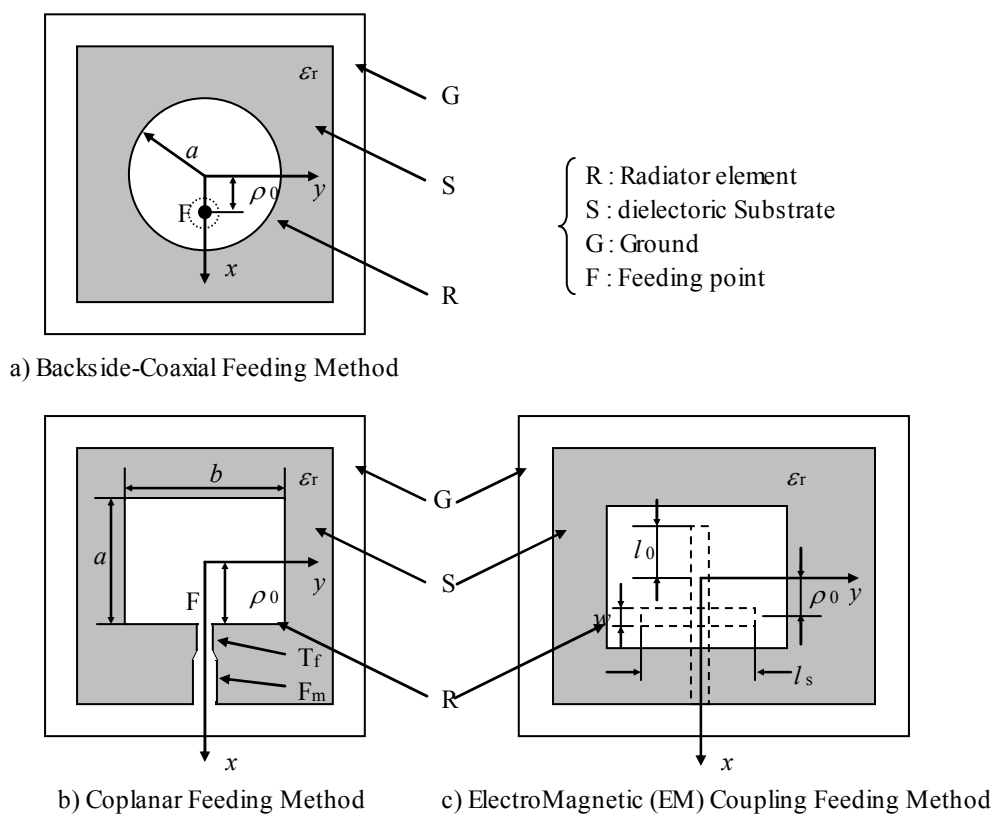
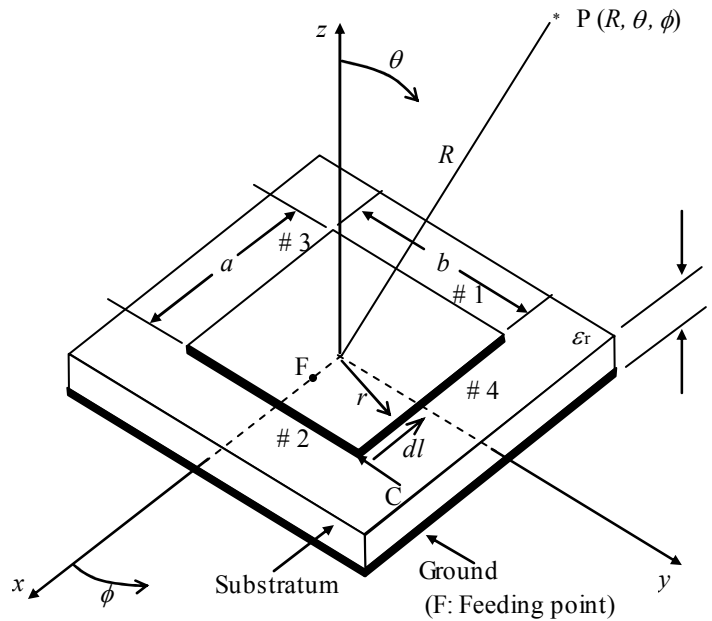


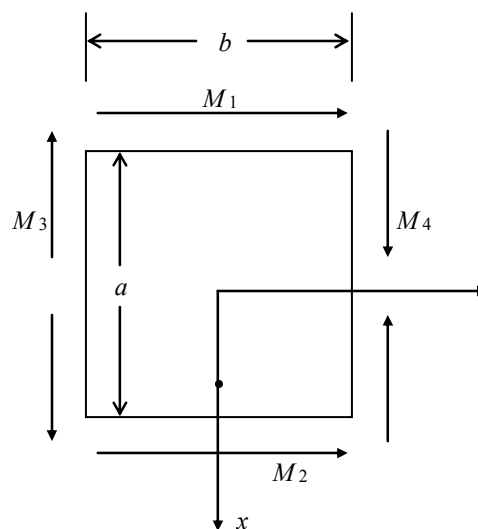
**Figure 3.3 Feeding Methods of MSA Element**

### 3.2.3 Interior Electromagnetic Field of Rectangular MSA

Figure 3.4 shows the analysis model of the inner electromagnetic field of a rectangular MSA. When the substrate thickness  $t$  is enough smaller than the free-space wavelength  $\lambda_0$  ( $k_0 t \ll 1$ ;  $k_0$  is a free-space wavenumber),  $TM_{mn0}$  wave is excited; it has an electric field element only to the direction of  $t$  (z direction).<sup>7</sup>



a) Coordinate System



b) Example of Magnetic Current

**Figure 3.4 Rectanglar MSA and its Coordinate System**

The electromagnetic field of this  $TM_{mn0}$  wave is expressed by follow wave equation:

$$\left(\nabla_t^2 + k^2\right)E_z = 0 \quad (\text{Interior region}) \quad (3.2)$$

$$\frac{\partial E_z}{\partial n} = 0 \quad (\text{Open boundary}) \quad (3.3)$$

where  $\hat{n}$  is outward unit normal vector at the open boundary and  $\nabla_t^2$  is  $(\partial^2/\partial x^2 + \partial^2/\partial y^2)$ .

When we separate variables of  $E_z$  element as  $E_z=X(x)Y(y)$  and of  $k$  element as  $k^2=k_x^2+k_y^2$  into  $x$  and  $y$  directions, and assign it to the equation (3.2):

$$\frac{1}{X} \frac{\partial^2 X}{\partial x^2} = -k_x^2 \quad (3.4)$$

$$\frac{1}{Y} \frac{\partial^2 Y}{\partial y^2} = -k_y^2 \quad (3.5)$$

where  $k_x=m\pi/a$  of a wavenumber in  $x$  direction and  $k_y=n\pi/b$  in  $y$  direction. by using the separation of variables,  $E_z$  element of  $TM_{mn0}$  wave is expressed by:

$$E_z = E_0 \cos\left(\frac{m\pi}{a}x + \frac{m\pi}{2}\right) \cos\left(\frac{n\pi}{b}y + \frac{n\pi}{2}\right) \quad (3.6)$$

$$k^2 = (k_x^2 + k_y^2) = \left[\left(\frac{m\pi}{a}\right)^2 + \left(\frac{n\pi}{b}\right)^2\right] \quad (3.7)$$

where  $E_0$  is an arbitrary number,  $k = \omega\sqrt{\varepsilon\mu}$  is the wavenumber in the dielectric, and  $m$  and  $n$  are arbitrary integers. Additionally, we assign this  $E_z$  to the Maxwell equation and consider the TM wave condition ( $H_z=0$ ), then we can find the interior electromagnetic elements of the rectangular MSA as:

$$\left. \begin{aligned} E_z &= \frac{V_0}{t} \cos\left(\frac{m\pi}{a}x + \frac{m\pi}{2}\right) \cos\left(\frac{n\pi}{b}x + \frac{n\pi}{2}\right) \\ H_x &= -\frac{j\omega\varepsilon}{k^2} \cdot \frac{n\pi}{b} \cdot \frac{V_0}{t} \cos\left(\frac{m\pi}{a}x + \frac{m\pi}{2}\right) \sin\left(\frac{n\pi}{b}x + \frac{n\pi}{2}\right) \\ H_y &= \frac{j\omega\varepsilon}{k^2} \cdot \frac{m\pi}{a} \cdot \frac{V_0}{t} \cos\left(\frac{m\pi}{a}x + \frac{m\pi}{2}\right) \cos\left(\frac{n\pi}{b}x + \frac{n\pi}{2}\right) \\ E_x &= E_y = H_z = 0 \end{aligned} \right\} \quad (3.8)$$

where  $V_0=tE_0$  is the peak voltage at the edge of the MSA element as a magnetic wall.

In the normal application of the rectangular MSA,  $TM_{100}$  or  $TM_{010}$  wave as the lowest order mode (basic mode) is important. The interior electromagnetic field of This  $TM_{100}$  wave can be find by the equation (3.8) as:

$$\left. \begin{aligned} E_z &= -\frac{V_0}{t} \sin\left(\frac{\pi}{a}x\right) \\ H_y &= \frac{j\omega\epsilon}{k^2} \cdot \frac{\pi}{a} \cdot \frac{V_0}{t} \cos\left(\frac{\pi}{a}x\right) \\ E_x = E_y = H_x = H_z &= 0 \end{aligned} \right\} \quad (3.9)$$

and Figure 3.5 shows the schematic of its electromagnetic distribution considering the edge effect.

Furthermore we can find the resonance frequency  $f_r$  of  $TM_{100}$  wave with assigning  $m=1$ ,  $n=0$  and  $k = \omega\sqrt{\epsilon\mu}$  as:

$$f_r = \frac{v_0}{2a\sqrt{\epsilon_r}} \quad (3.10)$$

where  $v_0$  is the light speed,  $\epsilon_r$  is the dielectric constant of the specimen substratum. When we calculate the resonance frequency of the rectangular MSA, we need to consider the fringing effect:

$$f_r = \frac{v_0}{2a_{\text{eff}}\sqrt{\epsilon_r}} \quad (3.11)$$

where  $a_{\text{eff}}$  is the equivalent side length and  $\epsilon_e$  is the effective dielectric constant, and they are expressed as:

$$\left. \begin{aligned} a_{\text{reff}} &= a \left\{ 1 + 0.824 \frac{t}{a} \cdot \frac{(\epsilon_e + 0.3)[(a/t) + 0.262]}{(\epsilon_e - 0.258)[(a/t) + 0.813]} \right\} \\ \epsilon_e &= \frac{\epsilon_r + 1}{2} + \frac{\epsilon_r - 1}{2} \left( 1 + 10 \frac{t}{a} \right)^{-0.5} \end{aligned} \right\} \quad (3.12)$$

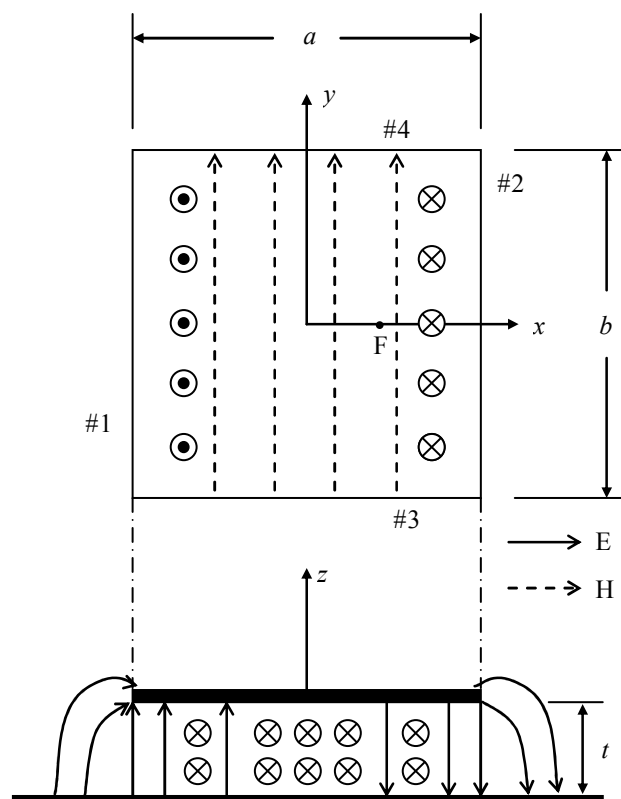


Figure 3.5 Schematic of Electromagnetic Distribution of  $TM_{100}$  wave

### 3.3 Theory of Rectifier Circuit Design

In order to develop the power conversion efficiency of a rectifier, we need its accurate output equivalent circuit model.<sup>13,14</sup> There are two independent approaches. Firstly, an approximate closed-form circuit was developed assuming an ideal diode and lossless circuit elements. The output equivalent circuit was obtained analytically. Secondly, a more precise computer-simulation model was used, and the load resistance and plotting the resultant output load line. In other researches, numerous rectifier circuits are possible, and a single shunt model diode rectifier circuit has proven most useful in the development work. Figure 3.6 shows an idealized equivalent circuit of this rectifier. The input filter should prevent any of the direct current (DC) and harmonic to flow back through the antenna resistance  $R_S$ , but allow current flow at the fundamental radio frequency (RF)  $\omega$ . The output filter should not only prevent alternating current (AC) components to appear across the load terminals but also allow harmonic currents to flow. In particular, the even harmonics should be allowed to flow since they have the property of having a zero average on each half cycle (harmonics are in phase with respect to fundamental). Therefore, the output filter should allow the even harmonics to flow without any voltage drop, prevent current flow at any of the odd harmonics, and allow DC current flow.

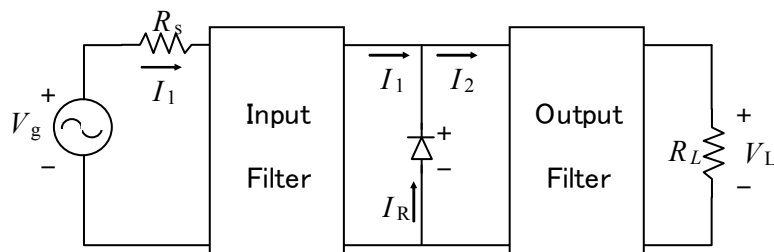


Figure 3.6 Simple Schematic of Rectifier Circuit with Input and Output Filters



### 3.3.1 Rectifier Circuit Model in Lumped Parameter System

There are two possible implementations of realizing filters with the above characteristics.<sup>13-16</sup> Figure 3.7 shows a method with using lumped circuit elements and satisfying these requirements. The elements  $L_3, C_3, L_5, C_5, \dots$ , form parallel resonant circuits. They are open circuited at the odd harmonics  $3\omega, 5\omega, \dots$ , respectively. The capacitor  $C_1$  is used for preventing DC flow as well as for series resonating  $L_3, C_3, L_5, C_5, \dots$ , at the fundamental frequency  $\omega$ . The  $L_2, C_2, L_4, C_4, \dots$ , elements in the output circuit are series resonant at the even harmonics  $2\omega, 4\omega, \dots$ , respectively. The inductance  $L_0$  is assumed to be large enough such that the current  $I_L$  is mainly DC. In that way the current  $I_L$  would consist of a DC plus even harmonics only.

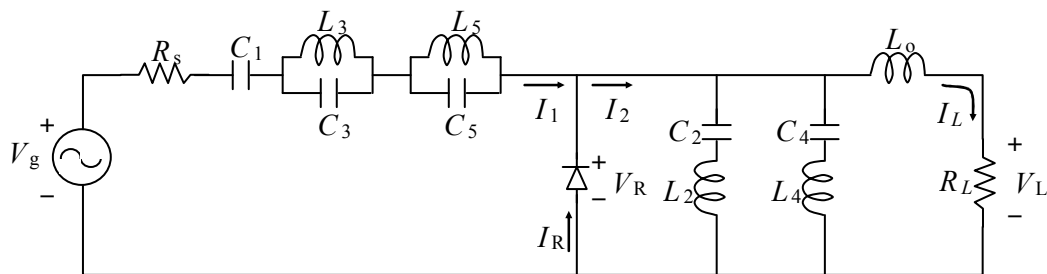


Figure 3.7 Schematic of Rectifier Circuit with Lumped-element Input and Output Filters

Figure 3.8 shows another possible method. In this circuit, the output filter consists of a non-dispersive transmission line terminated in a capacitor  $C_0$  in parallel with the load  $R_L$ ; it is a quarter wavelength long at the fundamental frequency. When  $C_0$  is enough large, the line can be considered to be at the load end and will appear at the diode terminals as an open circuit at  $\omega, 3\omega, 5\omega, \dots$  and as a short circuit at  $2\omega, 4\omega, \dots$ . Since their rectifier circuit analyses are ideal, we adopted the latter circuit design method in this thesis because of its simplicity. Additionally, I used only the capacitance  $C_1$  as the input filter for simplifying and miniaturizing the circuit patterns.<sup>16</sup> Figure 3.9 shows the rectifier circuit pattern and Figure 3.10 is its schematic. It consisted only of a chip condenser, a diode and micro-strip lines printed on the substratum.

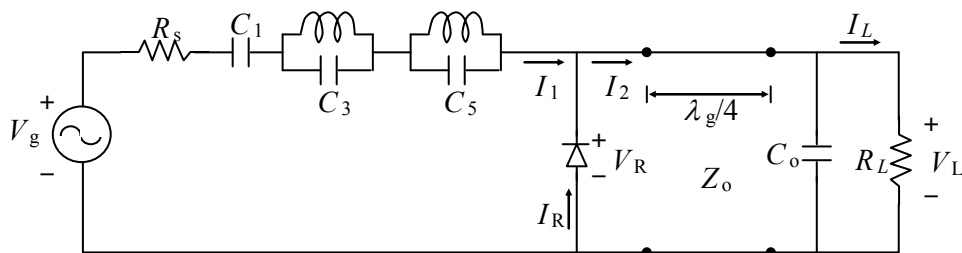


Figure 3.8 Schematic of Rectifier Circuit with a Transmission Line as Output Filter

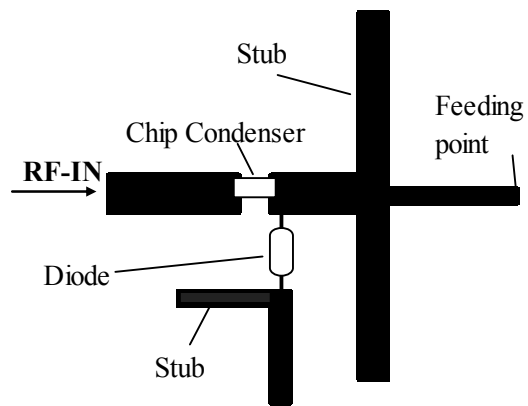


Figure 3.9 Rectifier Circuit Pattern

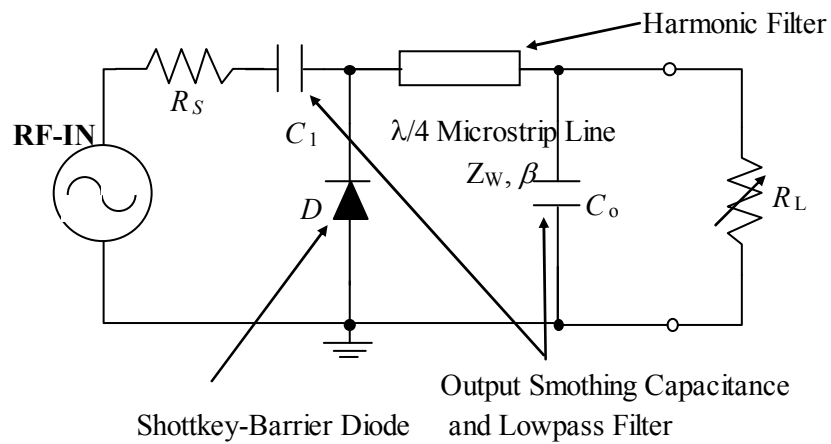


Figure 3.10 Schematic of Rectifier Circuit for Experiment

### 3.3.2 Matching of Input Impedance

The input line of the rectifier circuit was made as the micro-strip line. The line width  $W$  determines the characteristic impedance  $Z_w$  of the micro-strip line. Therefore,  $W$  is found by  $Z_w$  and is expressed as:<sup>17-19</sup>

$$W = W_0 - \Delta W \quad (3.13)$$

$$W_0 = \frac{8h \sqrt{\left\{ \exp \frac{Z_w \sqrt{\epsilon_r + 1}}{42.4} - 1 \right\} \frac{7 + \frac{4}{\epsilon_r}}{11} + \frac{1 + \frac{1}{\epsilon_r}}{0.81}}}{\exp \frac{Z_w \sqrt{\epsilon_r + 1}}{42.4} - 1} \quad (3.14)$$

$$\Delta W = \frac{t}{\pi} \ln \frac{4e}{\sqrt{\left(\frac{t}{h}\right)^2 + \frac{1}{\pi^2 \left(\frac{W_0}{t} - 0.26\right)^2}}} \quad (3.15)$$

where  $h$  is the thickness of the dielectric substrate,  $t$  is that of the conductor on the substrate,  $\epsilon_r$  is the dielectric constant,  $W_0$  is the equivalent width as  $t=0$ , and  $\Delta W$  is the offset of it.

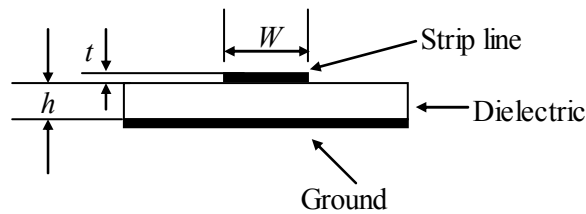


Figure 3.11 Structure of Micro-Strip Line

### 3.3.3 Design of Stub

In high-frequency circuit, a micro-strip stub with its length  $l_s < \lambda_g/4$  plays a role of a capacitor connected in parallel to the circuit.<sup>16,19,20</sup> Figure 3.12 shows the stub pattern and its equivalent circuit.

Its capacitance  $C_{eq}$  is expressed as:

$$C_{eq} = \left( \frac{1}{Z_C v'_p} - \frac{1}{Z_0 v_p} \right) l_s \quad (3.16)$$

where  $Z_0$  is the impedance of the transmitting line,  $Z_C$  is that of the stub,  $v_p$  is the phase speed on the transmitting line and  $v'_p$  is that on the stub. The phase speeds are also expressed as:

$$\begin{aligned} v_p &= f\lambda_g = \frac{c}{\sqrt{\epsilon_w}} \\ &= \frac{c}{\sqrt{\frac{\epsilon_r + 1}{2} + \frac{\epsilon_r - 1}{2\sqrt{1 + 10h/W}}}} \end{aligned} \quad (3.17)$$

$$\begin{aligned} v'_p &= f\lambda'_g = \frac{c}{\sqrt{\epsilon'_w}} \\ &= \frac{c}{\sqrt{\frac{\epsilon_r + 1}{2} + \frac{\epsilon_r - 1}{2\sqrt{1 + 10h/W_s}}}} \end{aligned} \quad (3.18)$$

where  $\epsilon_w$  and  $\epsilon'_w$  are the effective dielectric constants.

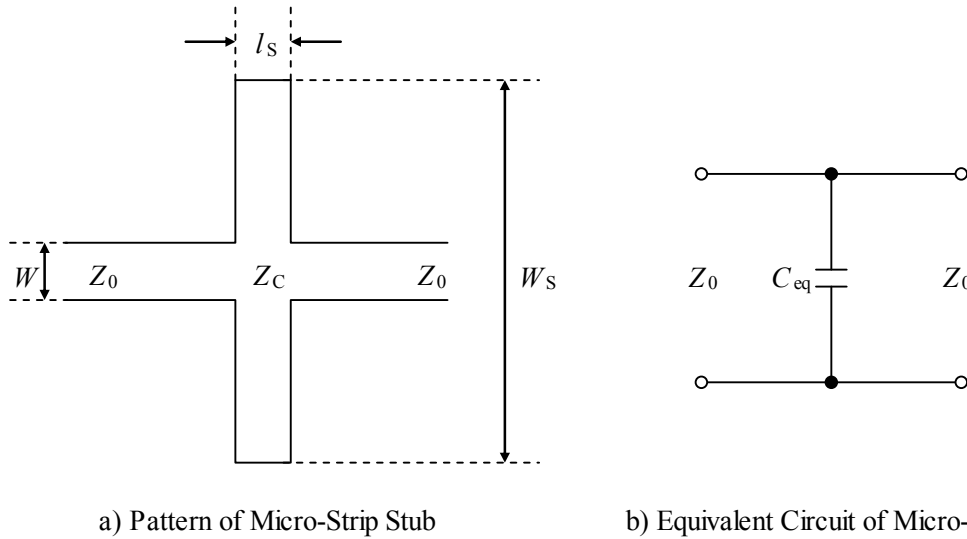


**Figure 3.12 Pattern and Equivalent Circuit of Micro-Strip Stub**

### 3.3.4 Output load-line Characteristics

Generally the input power  $P_a$  is expressed as:<sup>20</sup>

$$P_a = \frac{1}{8} \frac{|V_g|^2}{Z_0} \frac{|1 - \Gamma_g|^2}{|1 - \Gamma_g \Gamma_0 e^{-j2\beta l}|^2} \left(1 - |\Gamma_0 e^{-j2\beta l}|^2\right) \quad (3.19)$$

where  $\Gamma_0$  is the reflection coefficient of the load and  $\Gamma_g$  is that of the power source and  $\beta$  is the phase constant. Especially when their impedances matched each other,  $\Gamma_0=0$  and  $\Gamma_g=0$ , and then:

$$P_a = \frac{1}{8} \frac{V_g^2}{Z_0} \quad (3.20)$$

Since the circuit matched at  $Z_0=50\Omega$ , the voltage amplitude  $V_g$  of the power source with 10mW of the output power is:

$$V_g = \sqrt{8Z_0 P_a} = 2(V) \quad (3.21)$$

The rectifier circuit analysis is presented below. Since the current  $I_1(t)$  is only of the fundamental frequency and  $I_1(t)$  consists only of even harmonics, it follows that:<sup>13,14</sup>

$$V_L = \frac{\pi}{4} V_g - \frac{\pi^2}{8} R_S I_L \quad (3.22)$$

Figure 3.13 shows the characteristic of this equation and indicates follows; from the DC load terminals, the rectifier behave as a DC voltage source of amplitude  $(\pi/4)V_g$  and internal resistance  $(\pi^2/8)R_S$ .

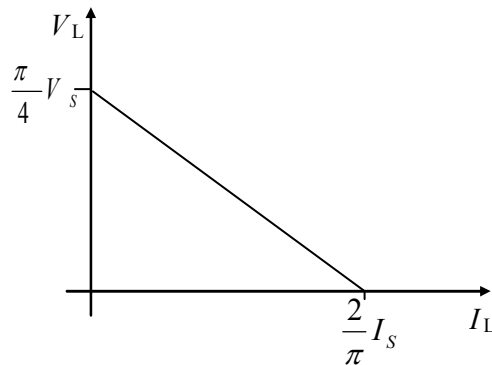


Figure 3.13 Relationship between DC equivalent circuit and load-line

Note that the voltage source is power-level dependent, but the equivalent output resistance is independent of RF power. Using this model, the optimum load for maximum DC load is:

$$(R_L)_{op} = \frac{\pi^2}{8} R_s \quad (3.23)$$

and the maximum dc power output is:

$$(P_L)_{max} = \frac{\left(\frac{\pi}{8} V_s\right)^2}{\frac{\pi^2}{8} R_s} = \frac{V_s^2}{8R_s} \quad (3.24)$$

which gives a 100 percent rectification efficiency.

This ideal efficiency has been achieved because it is assumed no losses in any of the circuit components or in the diode. However, since these losses can be minimized by choosing a rectifier diode with small forward drop and small-series resistance and high- $Q$  circuit elements, the closed-form conversion circuit model would be a good approximation to the characteristics of a high efficiency rectenna element.

Additional factors to be considered are the diode nonlinear depletion layer capacitance and package elements. Figure 3.14 shows the nonlinear V-I characteristic of a diode;<sup>21</sup> the forward current rises steeply over the forward voltage  $V_f$ , and the reverse current increases rapidly over the breakdown voltage  $V_R$ .

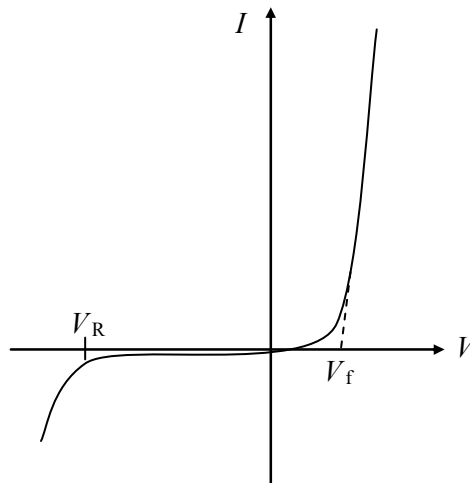


Figure 3.14 V-I Characteristic of Diode

### 3.3.5 Rectifier Circuit Model in Distributed Parameter System

In order to evaluate the effect of these additional factors, we need a detailed computer simulation model, or distributed parameter circuit model.<sup>13-15,22-24</sup> Figure 3.15 shows the equivalent circuit of a diode in the distributed parameter system. With these equivalent circuits, we could express that rectifier circuit pattern (Figure 3.9) in the distributed parameter system. Figure 3.16 shows the detailed computer simulation model of the rectifier circuit in the distributed parameter system. Although its characteristic was able to be analyzed with general circuit programs, such as SPICE, I could not. It is because the parameters of the diode and the micro-strip lines were not able to be identified; in the high-frequency circuit, the elements induce the capacitances, the reactances and the resistances, and the parameters of diode vary from production lot to production lot, or from element to element. Therefore, I optimized the rectifier circuit pattern from a pre-designed circuit by changing their parameters independently.

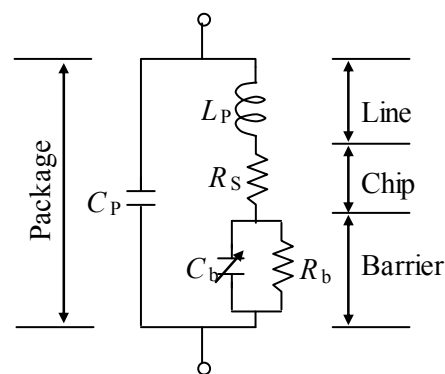


Figure 3.15 Equivalent Circuit of Diode

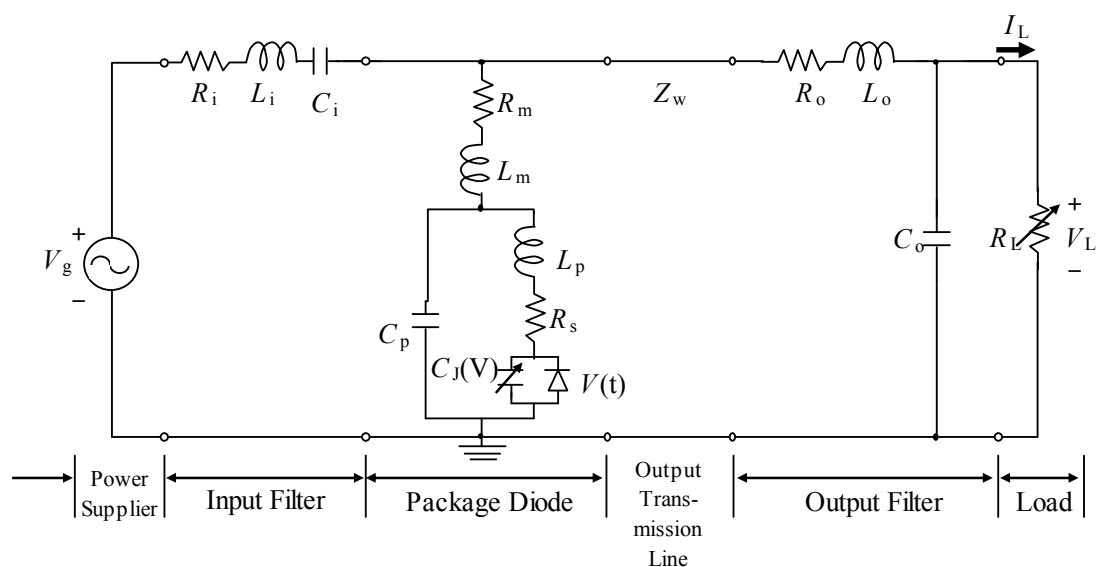


Figure 3.16 Detailed Schematic of Rectifier Circuit for Experiment

## Chapter 4 Experimental Apparatus

This chapter shows the power transmitting system, the power receiving system and others for the experiments and the demonstration.

### 4.1 Power Transmission System

Figure 4.1 shows the transmitting array antenna system. Microwave of 5.8 GHz was generated by an oscillator and was divided into five parts by a power divider. The phases of microwave parts without of the middle antenna were changeable individually with using four 6-bit digital phase shifters controlled by a PC. The driver amplifiers returned the power to level before phase shifting. Five FET amplifiers with the output power of 0.7W each mased into totally 3.5W output power.

Figure 4.2 shows the picture of it. Each microwave was guided to an antenna through a semi-flexible coaxial cable. Horn antennas were used as transmitting elements. Figure 4.3 shows the crisscross arranged antenna array; its array pitch  $d$  was 110mm and the diameter of the array  $D$  was 330mm. The beam was linearly polarized in the y-direction. Table 4.1 shows the specifications of this transmitting system.

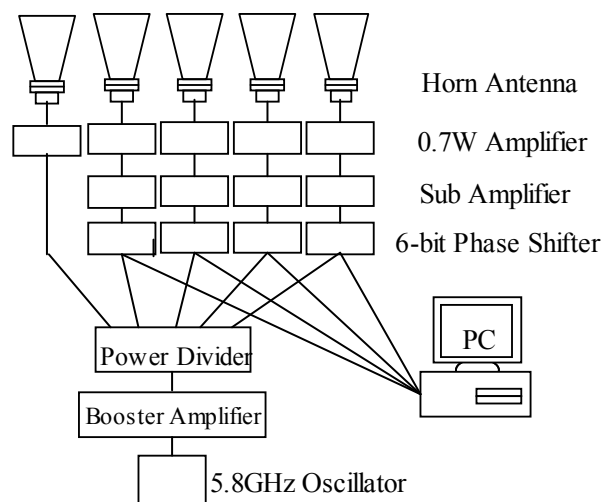


**Figure 4.1 Schematic of Transmitting Array antenna System**



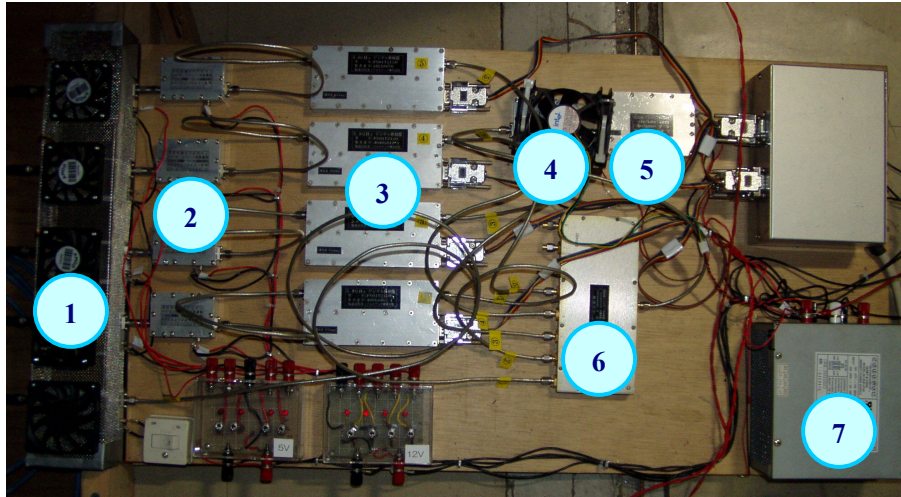


Figure 4.2 Picture of Transmitting System (1: Power Amplifiers, 2: Driver Amplifiers, 3: Phase Shifters, 4: Booster Amplifier, 5: Oscillator, 6: 8 Power Divider, 7: Power Source)

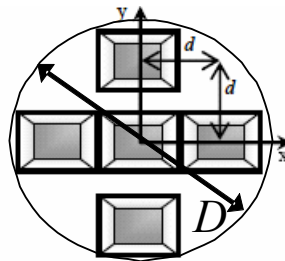


Figure 4.3 Arrangement of five antenna elements of the array

Table 4.1 Specifications of Transmitting Array Antenna System

Microwave Frequency	5.8GHz
Wavelength, $\lambda$	51.7mm
Total transmission Power, $P$	3.5W
Output Antenna	5 Horn antennas
Array pitch, $d$	110mm ( $d/\lambda=2$ )
Diameter of the array, $D$	330mm
Power Source	DC +5V, +12V

### 4.1.1 Oscillator

Microwave was produced by an oscillator (ArumoTech-OS00T2182) shown in Figure 4.4. Table 4.2 shows its specifications. This oscillator used the plate-tuning method with MOSFET (Metal Oxide Semiconductor Field Effect Transistor) for oscillating. Since it generates about the stable output power of 10 dBm, I used it for evaluating the handmade rectifier circuits by connecting them directly.

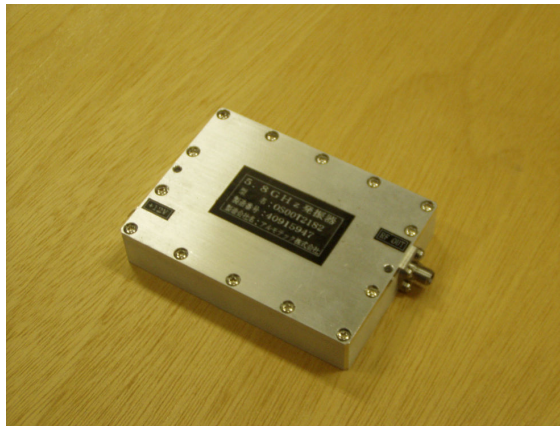


Figure 4.4 Picture of Oscillator

Table 4.2 Specifications of Oscillator

Model Name	OS00T2182
Output Microwave Frequency	5.8GHz
Output Power, $P_{osc}$	+10dBm $\pm$ 2dBm (10mW)
Output Connector	SMA-J
Power Source	DC +12V $\pm$ 0.5V

### 4.1.2 Power divider

Figure 4.5 shows a power divider (ArumoTech-PD00T2301). Microwave produced by the Oscillator was divided into 8 parts by the power divider, and each output of these parts was 1.25mW. In this experiment, we used five ports as the transmission lines. The unused three output lines were terminated with 50 $\Omega$  Terminators for suppressing the effects of the power reflection from one part to the other.

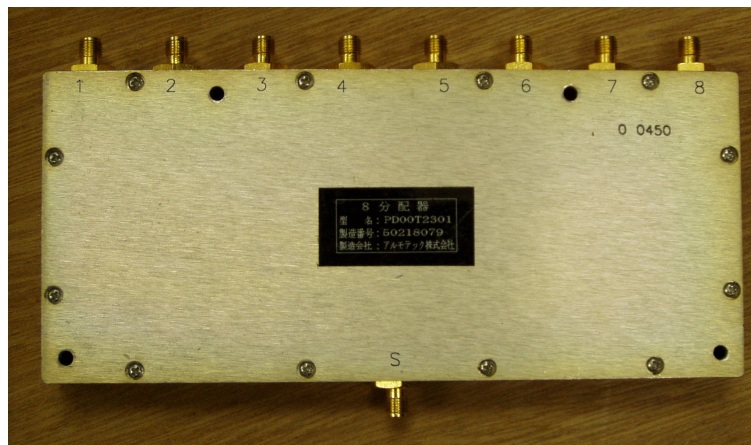


Figure 4.5 Picture of Power Divider

### 4.1.3 6-bit digital phase shifter

Figure 4.6 shows a phase shifter (ArumoTech-FS01T2150). We controlled the output phases with sending 6-bit signals from a computer to the phase shifters. Its phase resolutions were  $360^\circ/2^6 = 5.625^\circ$ . For example, the input signal is “010101”, the phase will be shifted by 118.125 degrees because of  $010101_{(2)} = (1*2^4 + 1*2^2 + 1*2^0)_{(10)} = 21_{(10)}$ . Depending on the set control bit the resulting phase might have a phase error. Table 4.3-4.6 shows the specifications of these four phase shifters.

This device shifted the phase by changing the physical length of the transmission line. Figure 4.7 shows the mechanism of the phase shifting. The phase shifter had the 6 elements each composed of two transmission lines with different length. The difference in length between the upper transmission line and the lower one corresponded to the amount of the shifted phase.

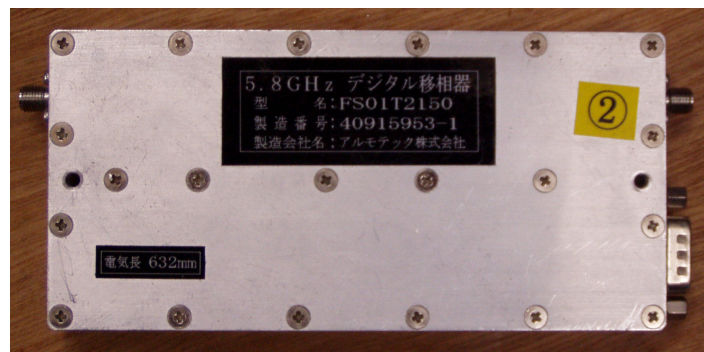


Figure 4.6 Picture of Phase Shifter

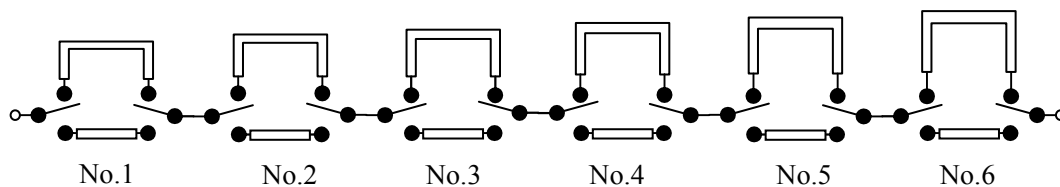


Figure 4.7 Mechanism of phase shifting

**Table 4.3 Specification of Phase Shifter No.2 (Lot No. 40915953)**

<b>Electrical Specification at 5.8GHz</b>				
<b>Bit No.</b>	<b>Amount of Shifted Phase [degree]</b>		<b>Insertion Loss [dB]</b>	<b>VSWR</b>
	<b>Default</b>	<b>Measured</b>	<b>29.0dB(TYP)</b>	<b>2.0(TYP)</b>
0	0	0	23.3	1.7
1	5.625±0.2	5.77	23.5	1.67
2	11.25±0.2	11.19	23.7	1.67
3	22.5±0.4	22.64	23.7	1.7
4	45.0±0.8	45.18	24.1	1.68
5	90.0±1.5	90.69	24.3	1.7
6	180±3	181.85	23.9	1.7

**Table 4.4 Specification of Phase Shifter No.3 (Lot No. 40405819-2)**

<b>Electrical Specification at 5.8GHz</b>				
<b>Bit No.</b>	<b>Amount of Shifted Phase [degree]</b>		<b>Insertion Loss [dB]</b>	<b>VSWR</b>
	<b>Default</b>	<b>Measured</b>	<b>29.0dB(TYP)</b>	<b>2.0(TYP)</b>
0	0	0	21.8	1.56
1	5.625±0.2	5.77	22.0	1.56
2	11.25±0.2	11.29	22.1	1.59
3	22.5±0.4	22.40	22.4	1.55
4	45.0±0.8	45.00	22.7	1.64
5	90.0±1.5	90.50	22.9	1.47
6	180±3	179.1	22.8	1.46

**Table 4.5 Specification of Phase Shifter No.4 (Lot No. 40405819-1)**

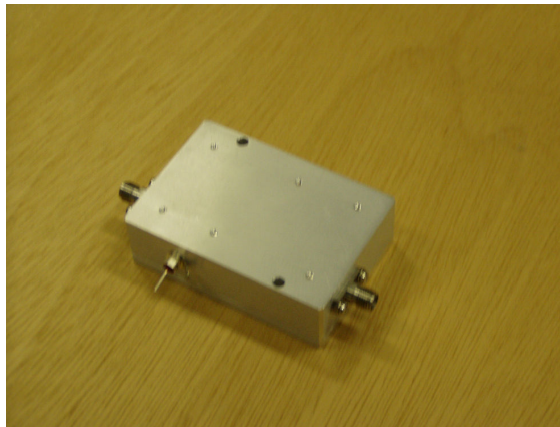
<b>Electrical Specification at 5.8GHz</b>				
<b>Bit No.</b>	<b>Amount of Shifted Phase [degree]</b>		<b>Insertion Loss [dB]</b>	<b>VSWR</b>
	<b>Default</b>	<b>Measured</b>	<b>29.0dB(TYP)</b>	<b>2.0(TYP)</b>
0	0	0	24.2	1.53
1	5.625±0.2	5.62	24.1	1.45
2	11.25±0.2	11.33	24.7	1.63
3	22.5±0.4	22.69	25.0	1.50
4	45.0±0.8	44.52	24.9	1.54
5	90.0±1.5	90.63	25	1.54
6	180±3	180.4	26.6	1.55

**Table 4.6 Specification of Phase Shifter No.5 (Lot No. 50218076)**

<b>Electrical Specification at 5.8GHz</b>				
<b>Bit No.</b>	<b>Amount of Shifted Phase [degree]</b>		<b>Insertion Loss [dB]</b>	<b>VSWR</b>
	<b>Default</b>	<b>Measured</b>	<b>29.0dB(TYP)</b>	<b>2.0(TYP)</b>
0	0	0	26.3	1.72
1	$5.625 \pm 0.2$	5.73	26.6	1.72
2	$11.25 \pm 0.2$	11.26	26.6	1.72
3	$22.5 \pm 0.4$	22.6	26.9	1.73
4	$45.0 \pm 0.8$	45.2	27.1	1.67
5	$90.0 \pm 1.5$	89.5	27.2	1.68
6	$180 \pm 3$	179.2	26.9	1.35

#### 4.1.4 Driver amplifier

Figure 4.8 shows a driver amplifier (ArumoTech-AP01T2149). The driver amplifier recovered the power loss generated by the phase shifter. This was set after the phase shifter and before the power amplifier. Table 4.7 shows the specification of the driver amplifier.

**Figure 4.8 Picture of Driver Amplifier****Table 4.7 Specification of Driver Amplifier**

Model Name	AP01T2149
Frequency Range	0.5~6GHz
Output Power, $P_{osc}$	+30dB or more
Input and Output Connector	SMA-J
Power Source	DC +12V $\pm$ 0.5V

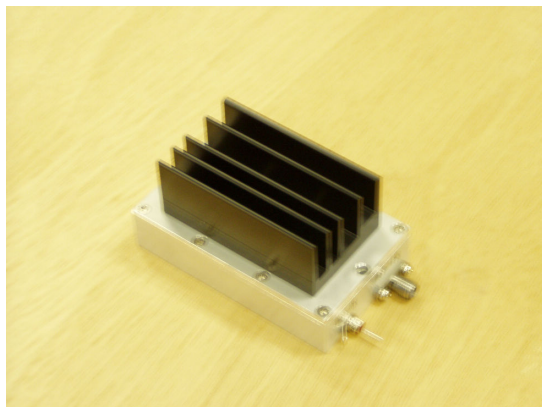
#### 4.1.5 Power amplifier

Figure 4.9 shows a power amplifier (ArumoTech-OS00T2182). It was a FET based amplifier for boosting the signal power to the desired output level finally, about 0.7W. Table 4.8 shows the specifications of the power amplifiers. This output power determined the total transmitting power from the horn antennas. The total amount of output power through the power amplifiers was 3382.1mW.

The output power level of all five used amplifiers should ideally be the same in order to obtain an even power distribution over all horn antennas, then the output power levels varied within a range of  $\pm 0.6\text{dBm}$  ( $\pm 10\text{mW}$ ). Figure 4.10 shows characteristic of one of the amplifiers, Amp. No. 1. The output powers of the amplifiers were saturated at about 28dBm. We used them at about the upper limit of the output power.

The power amplifiers generated heat from the heavily-loaded FET, and then the heat caused the dumbing down and unstable power supply of the devices. Although fins were installed on them for cooling, they were not enough. Therefore we installed the CPU fans over the devices for cooling forcibly.

Figure 4.11 shows the experimental result; cooling in 30 minutes, and then no cooling in 10 minutes. The temperature of the power amplifier stabilized in five minutes after the cooling start, and the output power also did in 15 minutes. In addition, the temperature became higher and the output power did lower rapidly as soon as we stopped the cooling. Therefore we decided to experiment after the 15 minutes' initial run.



**Figure 4.9 Picture of Power Amplifier**

**Table 4.8 Specification of Power Amplifiers**

No.	1	2	3	4	5
Model Name	OS00T2182				
Frequency Range	5.8GHz				
Input Power, $P_{pa\_in}$ [dBm]	+2.60	+11.24	+12.10	+10.93	+8.64
Output Power, $P_{pa\_out}$ [dBm]	28.31	28.29	28.26	28.29	28.36
Amplifier Gain [dB]	25.29	17.05	16.16	17.36	19.72
Input and Output Connector	SMA-J				
Power Source	DC +5V				

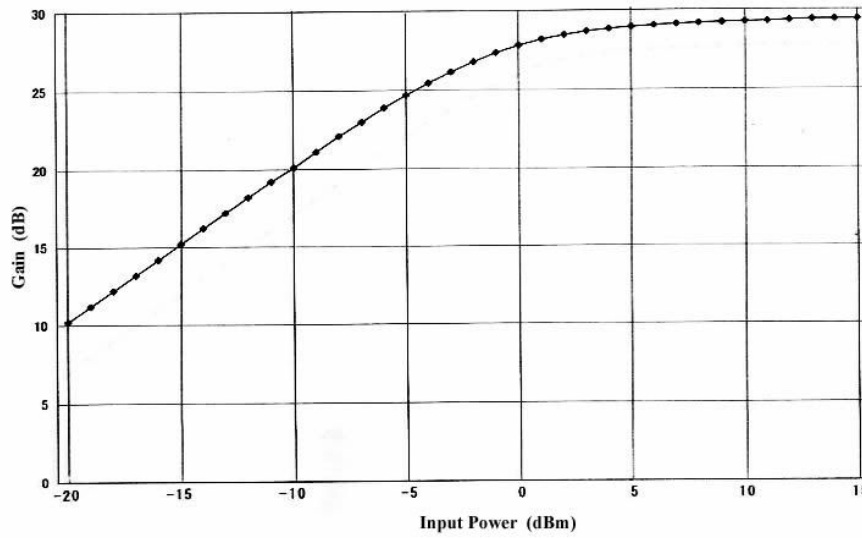


**Figure 4.10 Characteristic of Power Amplifier**

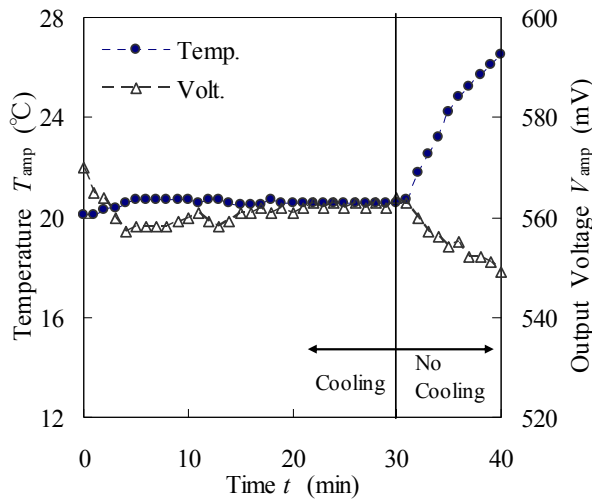


**Figure 4.11 Relationship of Temperature and Output Voltage of Power Amplifier**



#### 4.1.6 Booster amplifier

Figure 4.12 shows a booster amplifier (ArumoTech-AP00T2388). This device installed after the oscillator and before the power divider, and boosted the input power by 4.5dB. Without the booster amplifier, the output power of the power amplifiers often fluctuated due to the differences in phase attenuations at the commanded phases or other unidentified factors. The role of this device was to boost the input power to the power amplifiers enough for them to be reliably saturated. Table 4.9 shows the specification of the booster amplifier.

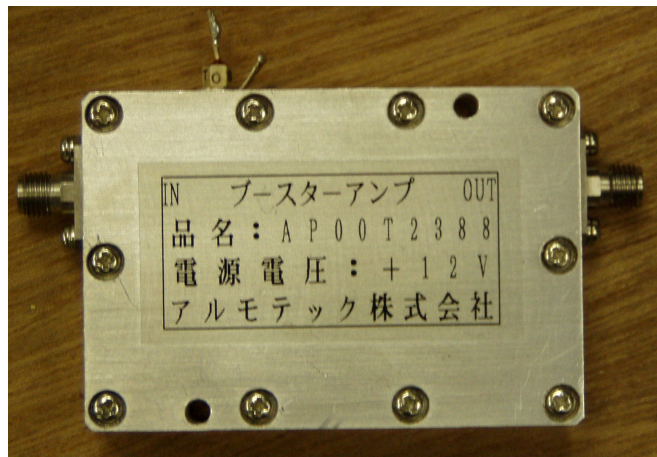


Figure 4.12 Picture of Booster Amplifier

Table 4.9 Specification of Booster Amplifier

Model Name	AP00T2388
Frequency Range	5.8GHz
Amplifier Gain	4.5dB (at 10mW input)
Input and Output Connector	SMA-J
Power Source	DC +12V ± 0.5V

#### 4.1.7 Horn antenna

Figure 4.13 shows the picture of a horn antenna and Figure 4.14 shows the size of the horn antenna. Its input plane size was  $\Delta x=40\text{mm}$  and  $\Delta y=20\text{mm}$  exit plane size was  $\Delta x=110\text{mm}$  and  $\Delta y=81\text{mm}$ .

The select of the antenna type for transmission mainly depended on two factors: the gain (or directivity) of the antenna and its polarization characteristics. Since the target had only a limited area available for receiving the transmitted energy, a high directivity of an antenna was desirable. Two prerequisites were needed for a high directivity. One was a large effective aperture size and the other was a uniform phase front at the aperture plane. The uniformity of the phase front also had an indirect effect on the aperture size and therefore on the directivity. The absolute gain  $G_a$  of a horn antenna was expressed as:<sup>8</sup>

$$G_a = 10 \log \left( \frac{4\pi \Delta x \cdot \Delta y}{\lambda^2} \right) \times \eta \quad (4.1)$$

where the aperture efficiency was 0.8 and the aperture size  $A_e$  was  $0.11 \times 0.081 = 0.00891 \text{ m}^2$ . This gives the  $G_a$  of this thesis was about 15.17dBi.

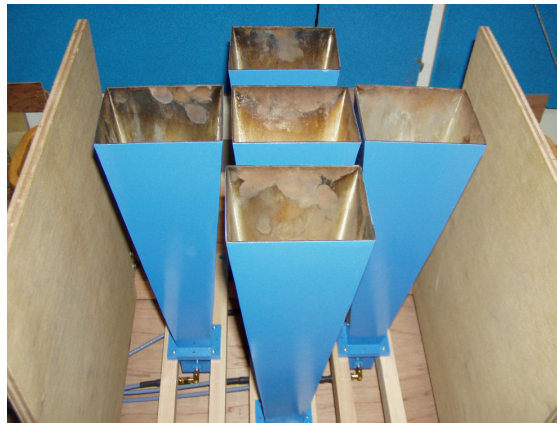


Figure 4.13 Picture of Horn Antenna

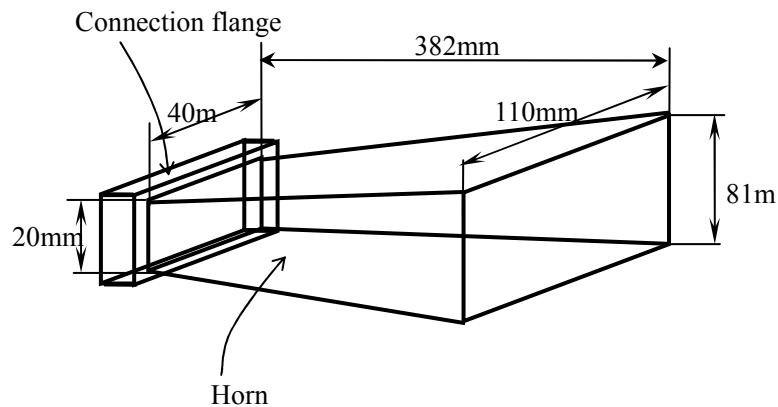


Figure 4.14 Size of Horn antenna

## 4.2 Power Receiving System / Measurement Apparatus

Figure 4.15 shows the power receiving system. It composed of antennas, rectifiers, an open/load switching unit and an oscilloscope. The microwave transmitted by the power transmitting system was received by the antennas, and was converted to DC power by the rectifiers, and was loaded by the open/load switching unit and was measured as the output voltage by the oscilloscope.

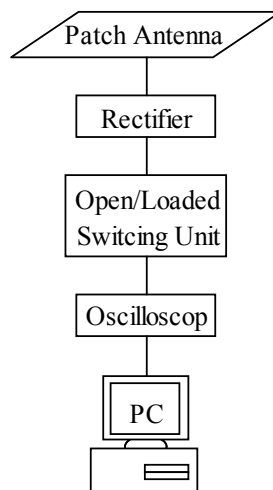


Figure 4.15 Schematic of Power Receiving System

### 4.2.1 Patch antenna

Figure 4.16 shows a patch antenna (ArumoTech). We used it as a standard receiving antenna. Its shape was a rectangle and its characteristic impedance was matched in  $50\Omega$ .

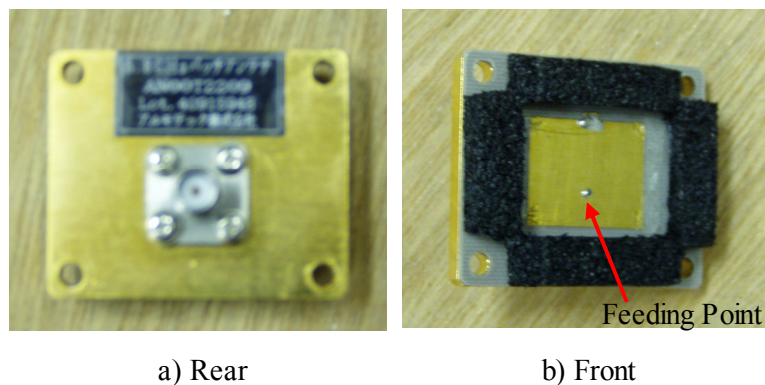


Figure 4.16 Picture of Patch Antenna

### 4.2.2 Rectifier

Figure 4.17 shows a rectifier (Pasternack Enterprises, Inc.-PE8016). We used it as a standard rectifier. Figure 4.18 shows the characteristic of the rectifier; the relationship between the input power  $P_{in}$  and the output voltage  $V_{out}$ . The curve in this graph was the fitted curve of this relationship and the input power  $P_{in}$  was calculated back with the output voltage  $V_{out}$  by:

$$P_{in} = 1.8166 \times 10^{-8} \cdot V_{out}^3 - 1.4833 \times 10^{-5} \cdot V_{out}^2 + 1.2969 \times 10^{-2} \cdot V_{out} \quad (4.2)$$



Figure 4.17 Picture of Rectifier

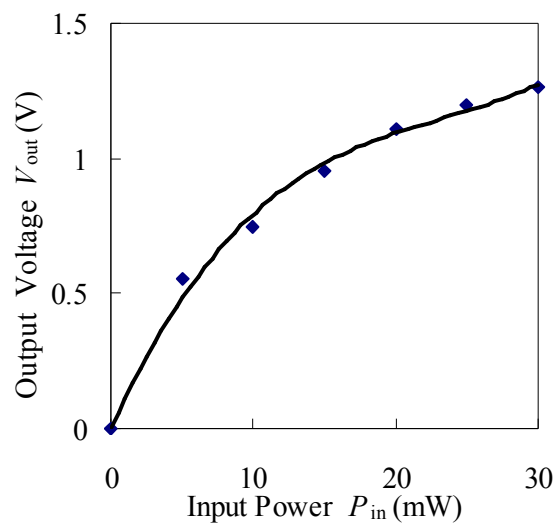


Figure 4.18 Characteristic of Rectifier

### 4.2.3 Open/Load switching unit

Figure 4.20 shows a open/load switching unit, and Figure 4.20 shows the schematics of the device. It installed after the rectifier and before the oscilloscope. It was able to switch between the open circuit mode and the loaded circuit mode. It had an analog linearly-variable resistance element in the range 2-4500 $\Omega$ . We were able to measure the open output voltage  $V_o$  in the open circuit mode (Figure 4.20 b)), and the loaded output voltage  $V_L$  and the Voltage  $V_i$  for calculating the current in the loaded circuit mode (Figure 4.20 b)).

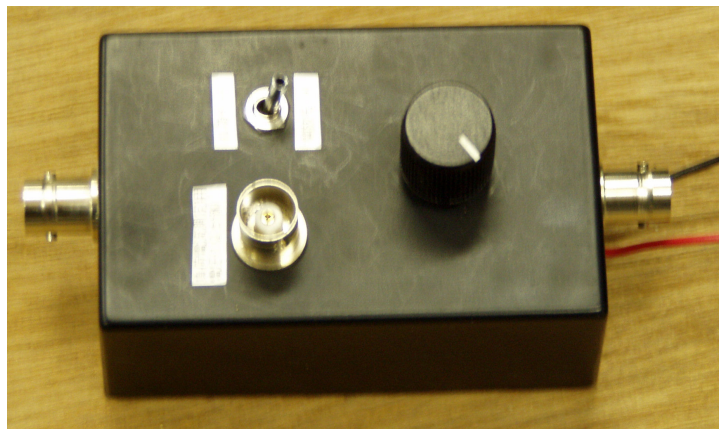
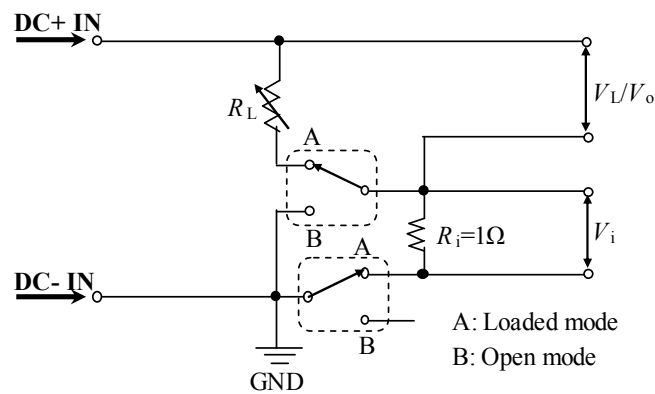
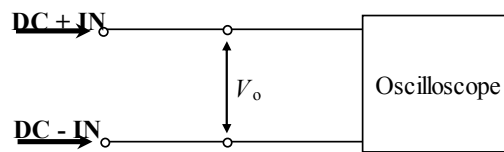


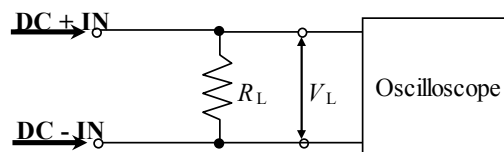
Figure 4.19 Picture of Open/Load Switching Unit



a) Circuit Schematic



b) Open circuit



c) Loaded circuit

Figure 4.20 Schematics of Load/Open Switching Unit

#### 4.2.4 Oscilloscope

Figure 4.21 shows oscilloscopes (Keyence-NR-2000, Keyence-NR-110). Although we measured the data with NR-2000 in the early phase of our experiment, we replaced it by NR-110 in the later phase due to circumstances beyond our control. Table 4.10 shows the specifications of the oscilloscopes. It measured the output voltage from the rectifier and sent the data to a computer for saving and analyzing.

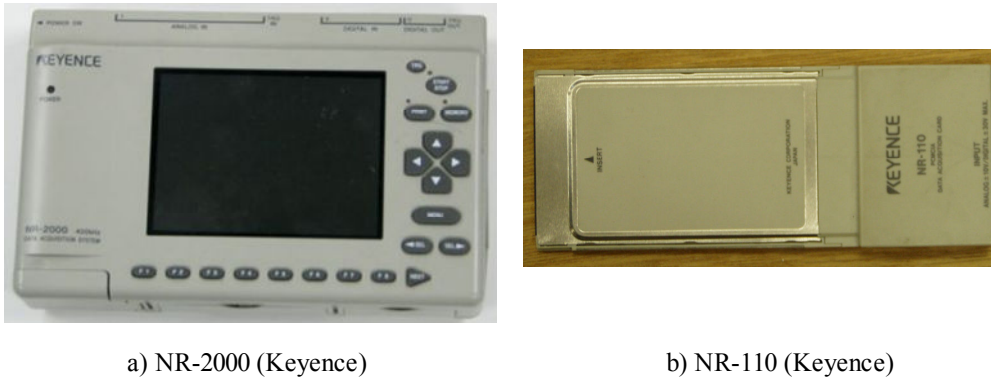


**Figure 4.21 Pictures of Oscilloscopes**

**Table 4.10 Specifications of Oscilloscopes**

Model Name	NR-2000	NR-110
Ch.	16ch(Single), 8ch(Differential)	16ch(Single), 8ch(Differential)
Resolution [bit]	14	14
Range [V]	10, 5, 2.5, 1, 0.5, 0.25	10, 5, 2.5
Gain	x1	x1 / x10
Input Impedance [MΩ]	1 (±1%)	1 ~
Max. Sampling Freq. [kHz]	400	50
PC Interface	USB 1.0 ~	PCMCIA2.1 / JEIDA4.2 ~

### 4.3 Experimental Setup and Others

I measured on a mounting structure surrounded by flat tile ferrite absorber. Additionally, I made rectenna elements of glass-epoxy substrate. In this section, I describe about the mounting structure and others for experimenting or demonstrating.

#### 4.3.1 Mounting structure

Figure 4.22 shows a mounting structure for the receiving modules. It was made of wood and thermoplastics. It consisted of a large wooden framework and a traverse stage enabling the receiving modules to slide smoothly in the y-axis direction. The framework was surrounded by flat tile ferrite absorber for reducing the reflection effect. The mounting structure was designed to make measurements in Cartesian coordinates. It allowed for continuous movement in the y-axis and discrete step movement in the other two axes. The movable ranges were:  $x: \pm 290(\text{mm})$ ,  $y: \pm 400(\text{mm})$ ,  $z: 235 + 100n (\text{mm}) <n = [0, 11]>$ .

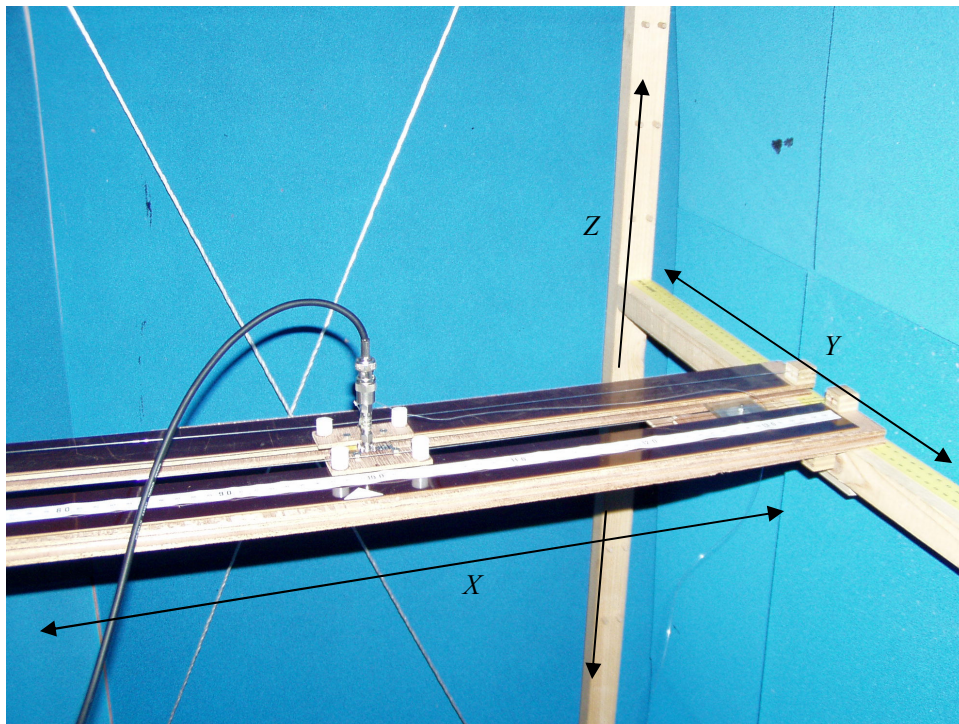


Figure 4.22 Picture of Mounting Structure



### 4.3.2 Substrate

In the experiments, I used glass-epoxy substrate FR-4 (Sanhayato Corp.). Table 4.11 shows the specification. We used its dielectric constant of 4.7 and its dielectric dissipation factor for calculation of 0.020. The substrate was pre-coated with photosensitive paint and left the antenna-patterns coating by developing. Then the unnecessary copper area was removed by substrate etching.

**Table 4.11 Specification of Substratum**

Material	Glass-Epoxy (FR-4)
Dielectric Constant $\epsilon_r$	4.5~4.8 (1MHz)
Dielectric Dissipation Factor $\tan\delta$	0.015~0.020 (1MHz)
Dielectric Thickness $h$ [mm]	1.6
Conductor Thickness $t$ [ $\mu\text{m}$ ]	35

### 4.3.3 Electrical Motor for Demonstration

Figure 4.23 shows a electrical motor for the power transmission demonstration and Table 4.12 is its specification. Although It was installed the AERO SOARER (TOMY Company Ltd.), the manufacture was not identified. Since it was able to operate with low electric power, I adopted it for the demonstration.

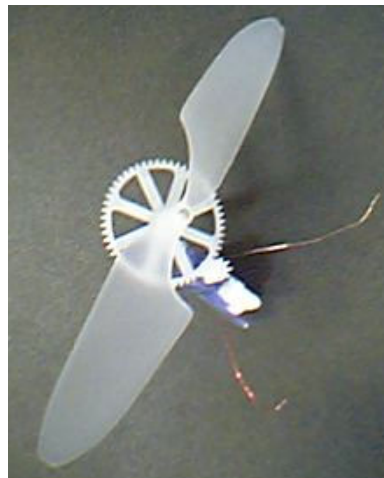


Figure 4.23 Picture of Electrical Motor

Table 4.12 Specification of Electrical Motor

Size	Glass-Epoxy (FR-4)
Min. Operating Voltage $V_{\min}$ [mV]	200
Min. Operating Current $I_{\min}$ [mA]	6
Inertial Resistance $R_L$ [ $\Omega$ ]	33
Rated Voltage $V_{\text{rat}}$ [V]	2.0
Rated Current $I_{\text{rat}}$ [mA]	60

## Chapter 5

### Measurement Results and Discussions

This chapter shows the measurements results of the experiments and discussions about the polarity-free antennas and the rectifier circuit patterns and the demonstration with the rectenna array.

#### 5.1 Polarity-Free Antenna

##### 5.1.1 Polarity-Free Antenna Designing

I designed some pattern of antenna by using a reference to circularly-polarized antenna. Figure 5.1 shows the patterns I made: (a) is square, (b) is rectangle, (c) is circle, (d) is octagon, (e) is chamfered a pair of opposing-corners of square by 45 degrees (ACPW, antenna for circular polarized wave), (f) is chamfered a pair of opposing-corners of square circularly (Leaf type), (g) is chamfered a pair of both end-corners of square circularly (Bathtub type) and (h) is chamfered all corners of square circularly. I also designed the different pattern in size of chamfering ratio  $r/a$  from 17% to 50%. Figure 5.2 shows the MSA array substrate. Each antenna on the substrate was feeded to the standard rectifier PE8016 by SMA-J connectors. Since the load resistance did not affect the antenna characteristic, we measured and discussed it by the output open voltage. After this, although I argue about the excerpted data, I show all data in Appendix.

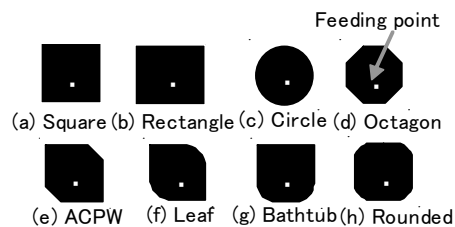


Figure 5.1 Antenna Patterns

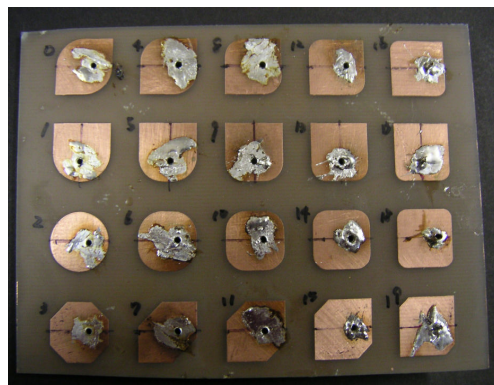
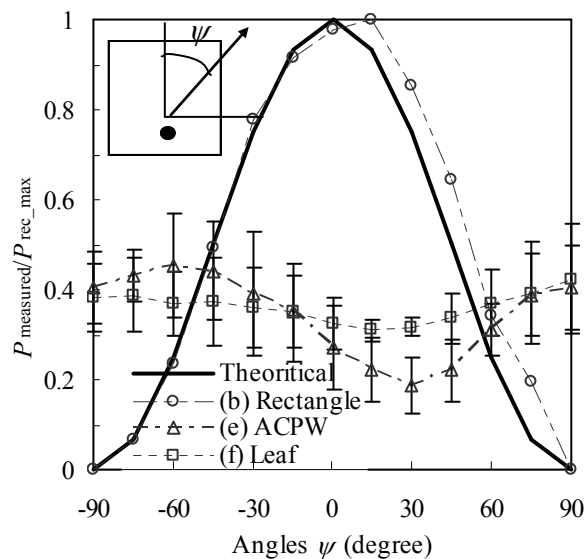


Figure 5.2 Picture of Handmade MSA Patterns

### 5.1.2 Effects of Antenna Patterns

I measured the power conversion efficiency as a function of antenna angle  $\psi$ . Figure 5.3 shows the angle dependency characteristics of some excerpted antenna patterns. MSAs had normally the polarization characteristics like (b) rectangle; very high conversion efficiency around the horizontal angle to the antenna resonance direction, and very low or near zero around the vertical angle. The ACPW MSA had different characteristics from the normal MSA; low efficiency around the diagonal angle of chamfered corners, and high around the diagonal angle of not chamfered corners. Moreover, the Leaf MSA showed the almost flat angle dependency characteristic, smoother than the ACPW MSA.



**Figure 5.3 Angle Dependency Characteristics (Antenna Patterns)**

### 5.1.3 Effects of Chamfering Ratio

I experimented with changing the chamfering ratio  $r/a$  from 17% to 50%. Figure 5.4 shows the angle dependency characteristics about some excerpted chamfering ratios of the Leaf MSA. As seen in the figure, the chamfering ratio was one of the determining factors of the angle dependency characteristics of the MSA. As a result, the Leaf MSA at  $r/a=0.33$  was the best polarity-free characteristics; its power conversion efficiency was varied only 33% to 40% for the 360 degree changes of  $\psi$ . Table 5.1 shows the specification of the Leaf MSA.

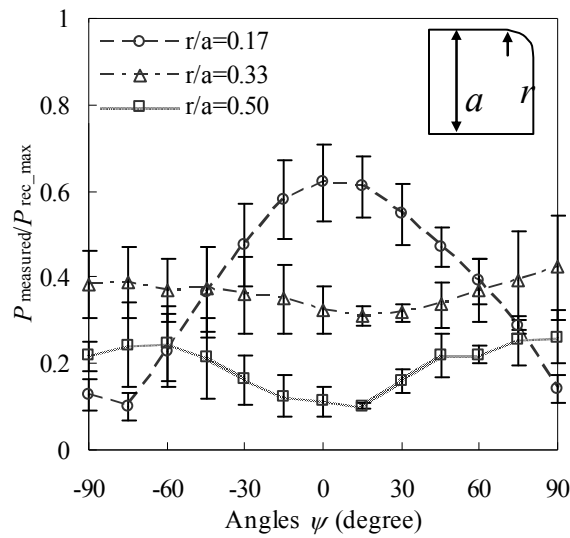


Figure 5.4 Angle Dependency Characteristics (Chamfering Ratios)

Table 5.1 Specifications of Best Polarity-Free MSA

Antenna Pattern	Leaf type
Chamfering Ratio $r/a$	0.33
Average	0.36
Max.	0.31
Min.	0.42

#### 5.1.4 Assumption and Simulation of Current Distributions on MSA

In this session, I discuss about the reason why the Leaf MSA showed the polarity-free characteristic. Since MSAs have normally the polarization characteristics, they have their own special resonance direction. However, the Leaf MSA showed the nearly-constant polarization characteristic in all angles of the incident wave polarization plane. Hereupon I assumed the following models.

First, we can obtain only the resonance direction ingredient of the incident microwave by using the normal rectangle MSAs. In turn, when the microwave with its power  $P_0$  was incident to the MSA at the angle  $\psi$  of its wave polarization to the antenna resonance direction, the obtainable power  $P_{rect}$  would be expressed as:

$$P_{rect} = P_0 \cos(\psi) \quad (5.1)$$

As seen in Figure 5.3, I found close resemblance between the measured data and the calculated.

Secondly, I discuss about the ACPW; it is chamfered a pair of opposing- corners of square by 45 degrees. The polarization plane of the transmitting wave from the ACPW rotates depending on its phase. From the antenna reversibility for transmitting and receiving, I guessed the resonance would depend on the polarization plane angle of the incident microwave when I used it as a receiving antenna.

Lastly, I discuss about the Leaf MSA. Its shape was almost the same as the ACPW; the difference was the chamfering pattern whether by 45 degrees or roundly. I assumed that the reflection on its edge would become more complex and the power resonated in the antenna resonance direction would be increased.

For follow-up of the above assumption, I simulated the interior electromagnetic field distribution with using the SONNET Lite (Sonnet Software Inc.). In this simulation, I analyzed the current distribution of some MSAs (square, ACPW, Leaf) for transmitting because of the limitation from its evaluation version. Figure 5.5 shows the analysis results. As seen in the figure, the resonance direction of the square MSA is constant, and that of the the ACPW and the Leaf MSA rotate with depending on the wave phases. The ACPW resonates the most at the antenna resonance direction, and the resonance become weak as the polarization plane rotates. The Leaf MSA resonates evenly around all of the polarization angles, though it does weaker than the ACPW at the antenna resonance direction. As a result, I assumed the Leaf MSA shows the polarity-free characteristic, the independent power receiving from the incident microwave polarization plane angles from this effect.

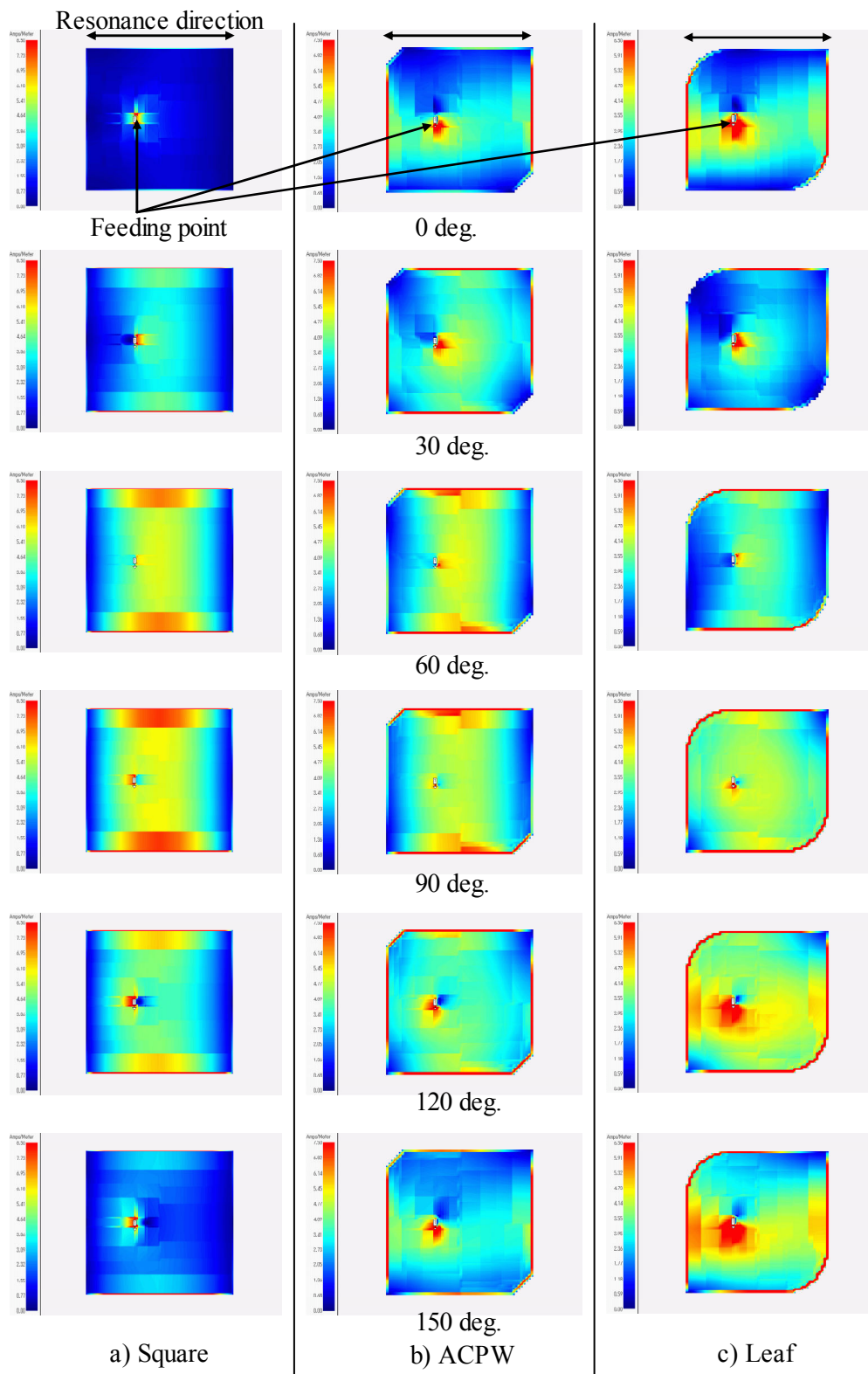


Figure 5.5 Current Distributions of MSAs (a: square, b: ACPW, c: Leaf)

### 5.1.5 Comparison with Unit of Multiple Dipole Antennas

To discuss the effectiveness of the Leaf MSA, I compare it with the unit of multiple dipole antennas. I assume that I use the size of the UMDA as a standard power receiving area  $A_{\text{std}}$ , and the input power  $P_{\text{in}}$  is transmitted within this area.

The effective area of the dipole antenna as the element of the UMDA is expressed as:

$$A_{\text{UMDA}_{\text{eff}}} = \frac{W_m}{P} = \frac{30\lambda^2}{R\pi} = 0.131\lambda^2 \quad (5.2)$$

With considering eight antennas within the area, the effective area as the unit is  $1.048\lambda^2=7[\text{cm}^2]$ , and the receivable power is  $7P_{\text{in}}/A_{\text{std}}$ .

The effective area of the MSA is expressed as the equation (3.12), and , with considering nine antennas within the area, the total effective area is about  $12.8[\text{cm}^2]$ , and the receivable power is about  $12.8 P_{\text{in}}/A_{\text{std}}$ .

Figure 5.6 shows the comparison result with considering above the effective area influences. As seen in this graph, I find the UMDA has a polarity-free characteristic because of its equability, but the conversion efficiency is very low. The characteristic of the Leaf MSA is similar to that of the UMDA , moreover, the conversion efficiency of the Leaf is higher than of UMDA. As a result, the SPFA method is more effective element for polarity-free than the UMA method for following reasons; as small size as one antenna element, good polarity-free characteristic, high conversion efficiency.

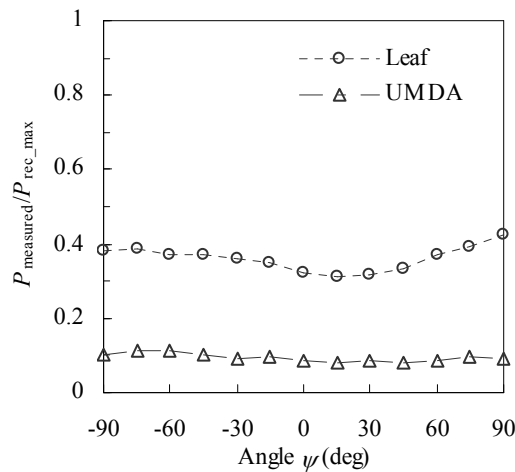


Figure 5.6 Comparison Leaf MSA with UMDA



## 5.2 Optimization of Rectifier Circuit

In designing rectifier circuit patterns, variable parameters are below:

- Type of Schottky Barrier Diode (SBD):  $D$
- Capacitance of chip condenser:  $C_0$
- Input width:  $W$
- Input length:  $l_{in}$
- Width between diode and ground:  $W_g$
- Length between diode and ground:  $l_g$
- Stub width after diode:  $W_S$
- Stub length after diode:  $l_S$
- Output transmission line (OTL) length:  $l_{tl}$
- Low Pass Filter (LPF) shape:  $W_C, l_C$
- Output width:  $W_{out}$
- Output length:  $l_{out}$

Figure 5.7 shows their parameters on the pattern. The parameters of  $W, l_{tl}$  are predetermined by the theory;  $W=2.83\text{mm}$  at 5.8GHz for impedance matching, and  $l_{tl}=\lambda_g/4$  for output filter. Moreover, it was founded by the research in the Kyoto University that some parameters seldom affect the conversion efficiency;  $C_0, l_{in}, W_g, W_S, W_C, l_C, W_{out}$  and  $l_{out}$ . First I designed the standard rectifier circuit patterns. Table 5.2 shows its values and products. I experimented with varying the parameters independently and discuss the results below.

In following experiments, I connected the test rectifier circuit to the oscillator directly, and I measured the output voltage  $V_{measured}$  from the rectifier circuit with the oscilloscope. The wattage  $P_{measured}$  of the load is expressed as:

$$P_{measured} = \frac{V_{measured}^2}{R_L} \quad (5.3)$$

where  $R_L$  is the resistance value of the load. Since the input power  $P_{in}$  is given as 10dBm from the oscillator specification, the conversion efficiency of the rectifier circuit is found by:

$$\eta = \frac{P_{measured}}{P_{in}} \quad (5.4)$$

Thus, I calculated the efficiencies with changing the parameters.

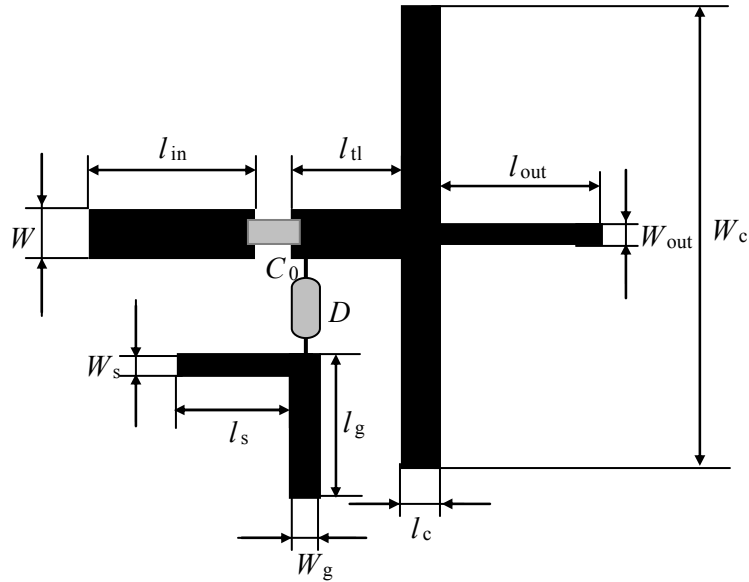


Figure 5.7 Schematic of Rectifier Circuit Pattern Parameters

Table 5.2 Parameters for Standard Rectifier Circuit Pattern

Parameters	Value / Product
$D$	1SS97 (NEC)
$C_0$ [pF]	33 (muRata-GRM42-6 SL 330J 50)
$W$ [mm]	2.83
$l_{in}$ [mm]	10.00
$W_g$ [mm]	1.50
$l_g$ [mm]	8.20
$W_s$ [mm]	1.00
$l_s$ [mm]	0
$l_{tl}$ [mm]	$6.67 (\lambda_g/4)$
$W_c$ [mm]	28.00
$l_c$ [mm]	2.00
$W_{out}$ [mm]	1.00
$l_{out}$ [mm]	10.00

### 5.2.1 Type of Schotkky Barrier Diode: *D*

The type of diode is one of the most effective parameters deciding the conversion efficiency. Since the reverse recovery speed is important factor as the diode of microwave rectifier circuit, I used some SBDs and experimented; 1SS97 (NEC), 1SS108 (HITACHI), 1SS281 (NEC). Figure 5.8 shows the load characteristic related to the SBD. As seen in the graph, 1SS281 achieved the best conversion efficiency. However, since 1SS281 had been discontinued and was hardly available, it was unsuitable for mass production of rectenna. 1SS97 was relatively available compared with 1SS281 though it was also the discontinued product, then I determined 1SS97 as the rectenna diode. In turn, for rectifying microwave, I suggest that the type of SBD with following characteristics will be suitable; low following voltage  $V_f$ , high breakdown voltage  $V_r$ .

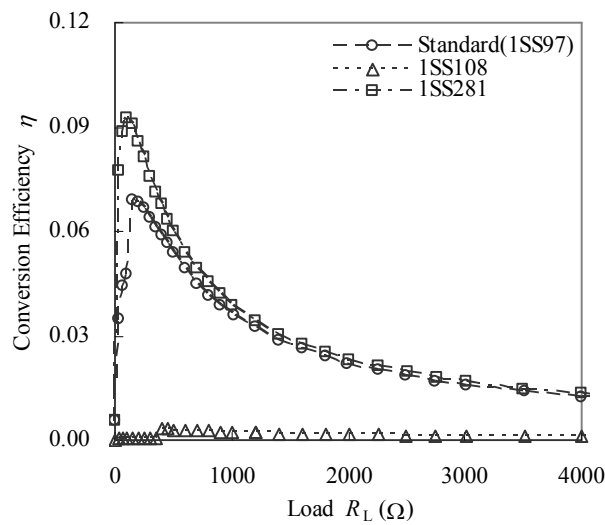


Figure 5.8 Load Characteristic related to SBD

### 5.2.2 Capacitance of Chip Condenser: $C_0$

The role of the chip condenser was smoothing the DC and preventing it from flowing to the RF input side. In these reasons, the chip condenser was acceptable if it had a certain value about over 1pF. I used the following values and experimented; 33pF (muRata-GRM42-6 SL 330J 50), 150pF (TDK-C3216X7R 151), 470pF (muRata-GRM42-6 B 471K 50). Figure 5.9 shows the load characteristic related to the capacitance of the chip condenser. As seen in the figure, the conversion efficiency is seldom related to the capacitance values, but to the manufactures or the packages of the chip condensers. However, there might be some peaks of the conversion efficiency at a certain capacitance value, therefore it is important to survey the conversion efficiencies at more capacitance values.

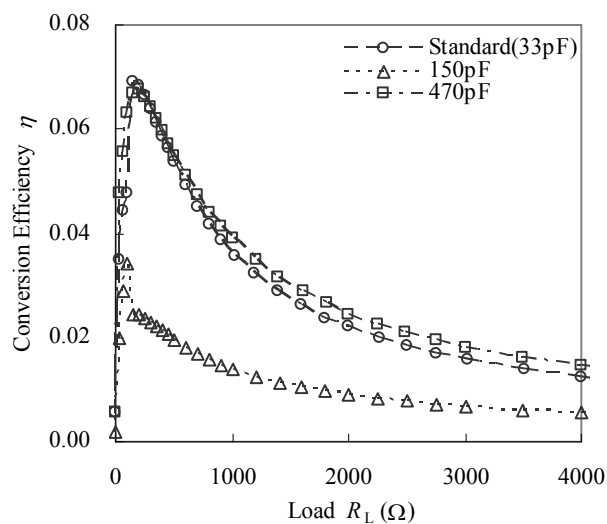


Figure 5.9 Load Characteristic related to Capacitance

### 5.2.3 Input Width: $W$

The input width is calculated as  $W=2.83\text{mm}$  by the equation (3.13-15). Although it is the determined parameter for impedance matching, it has a possibility of for changing the impedance by producing error. For considering the producing error effect, I made the pattern with a little different width  $W=3\text{mm}$  and experimented; its characteristic impedance was about  $48.4\Omega$ .

Figure 5.10 shows the effect from the width difference. As seen in this graph, the system was matched in the characteristic impedance of  $50\Omega$ , and when the actually produced patterns differed from the designed one, the losses of the efficiency happen; about 2% losses by the width difference of  $1.7\text{mm}$ . As a result, the improvement in the production accuracy is one of the important factors.

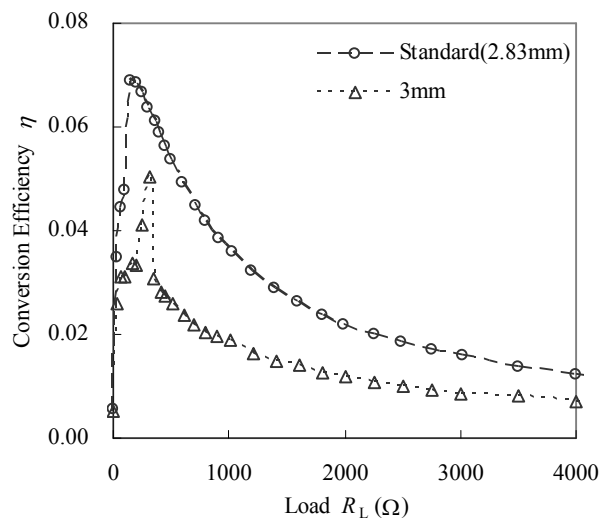


Figure 5.10 Load Characteristic related to Input Width

#### 5.2.4 Input Length: $l_{in}$

Since the input length was not related to the conversion efficiency theoretically, I adopted the value of  $l_{in}=10\text{mm}$ , about  $3\lambda_g/8$ , for the design simplicity. However, this length might affect the incident microwave propagation and cause the efficiency reduction because the element was located in the RF area before the diode. Thus, I considered it as a variable parameter and experimented.

Figure 5.11 shows the result. From this, the length is one of the key parameters determining the conversion efficiency, and there is an optimal value for the best efficiency. Moreover the efficiency reaches the minimum value at  $l_{in}=\lambda_g/2$  and the maximum at  $l_{in}=\lambda_g/4$ .

Generally, when the load is connected to the output terminal of a transmission line, the input impedance of the transmission line is expressed as:

$$Z_{in} = Z_0 \frac{Z_L + jZ_0 \tan \beta l}{Z_0 + jZ_L \tan \beta l} \quad (5.5)$$

where  $Z_0$  and  $Z_L$  are the characteristic impedances of the transmission line and the load, and  $\beta$  is the phase constant. When the line length is integer multiples of  $\lambda_g/2$ , or even multiples of  $\lambda_g/4$ ,  $\beta l = (2\pi / \lambda_g) \cdot (2n\lambda_g / 4) = n\pi$  ( $n$  is an integer of 0 and over), and (5.5) is represented as:

$$Z_{in} = Z_L \quad (5.6)$$

It means the input impedance is equal to  $Z_L$  when the line length is  $n\lambda_g/2$ .

When the line length is odd multiples of  $\lambda_g/4$ ,  $\beta l = (2\pi / \lambda_g) \cdot [(2n+1)\lambda_g / 4] = (2n+1)\pi / 2$ ,  $\tan \beta l = \infty$ , and (5.5) is represented as:

$$Z_{in} = Z_0^2 / Z_L \quad (5.7)$$

It means that the relationship between  $Z_0$  and  $Z_L$  is the inversion.

Normally, it is ideal that the transmission length is  $n\lambda_g/2$  because the input impedance is represented as the load impedance for matching the circuit impedances. However, in this experiment, I connected the microwave power source, or the oscillator, to the rectifier circuit by SMA connector. Without considering the connector line length, the efficiency should be the maximum value at  $l_{in}=\lambda_g/2$ , but it was actually not. Thus, I consider bellow; the line length from the oscillating source or the input terminal of the rectifier connector to the RF feeding point is already  $(2n+1)\lambda_g/4$ , and the total length become  $n\lambda_g/2$  with the input length of  $\lambda_g/4$ . As a result, the efficiency reaches the maximum value at  $l_{in}=\lambda_g/4$  and the minimum at  $l_{in}=\lambda_g/2$ . Furthermore, we need to readjust this parameter when we combine the rectifiers and the antennas as the rectennas. It is because the length from the RF feeding point of the antenna to that of the rectifier might not be  $n\lambda_g/4$ ; I guess it should be shorter than  $\lambda_g/4$ .

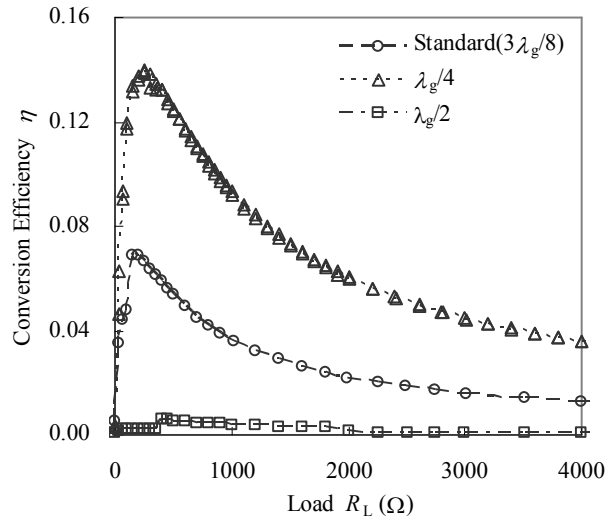


Figure 5.11 Load Characteristic related to Input Length

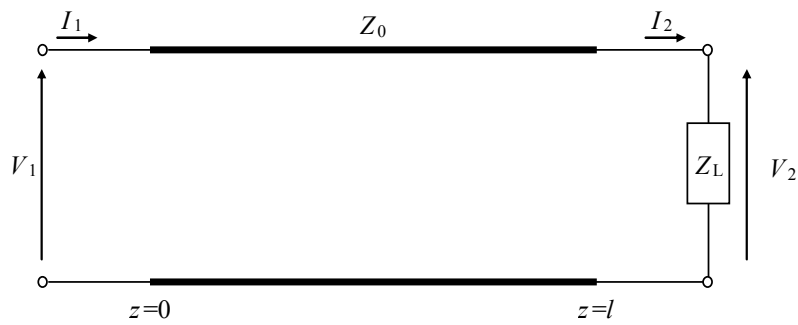


Figure 5.12 Schematic of 2 End Terminals of Distributed Parameter Line

### 5.2.5 Width between Diode and Ground: $W_g$

Since the width between the diode and the ground (D-G width) was also not related to the conversion efficiency theoretically, I adopted the value of  $W_g=1.5\text{mm}$  for the design simplicity. However, if the RF element exists in the D-G line, the impedance difference between the D-G line and ground would affect the efficiency. Thus, I surveyed the effect of the width  $W_g$ .

Figure 5.13 show the result. From this, I can say that there are hardly any effects of the width to the conversion efficiency. However, since the number of the surveyed elements is small, we should survey with more elements.

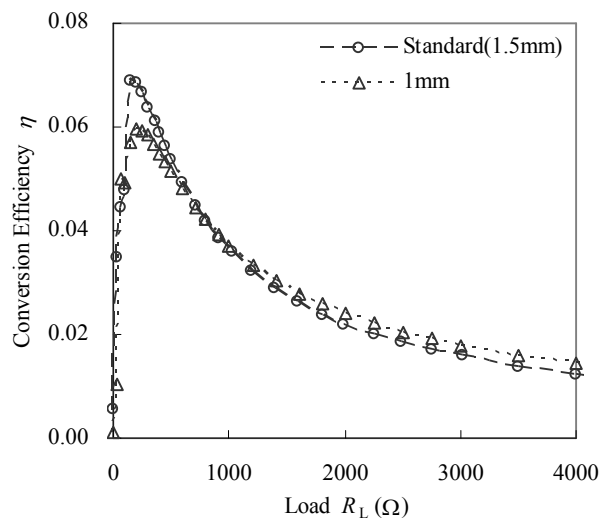


Figure 5.13 Load Characteristic related to D-G Width



### 5.2.6 Length between Diode and Ground: $l_g$

Since the length between the diode and the ground (D-G length) was also not related to the conversion efficiency theoretically, I adopted the value of  $l_g=8.2\text{mm}$ , about  $\lambda_g/5$ , for the design simplicity. However, if the RF element exists in the D-G line, the length would affect the efficiency. Thus, I surveyed the effect of the length  $l_g$  as well as the width  $W_g$ .

Figure 5.14 shows the result. From this, I can say the RF element reminded in the D-G line because this parameter has a great influence on the conversion efficiency. I discuss the effect by using the distributed parameter line model with the two end terminals and the equation (5.5).

Since one end terminal is connected to the ground, I regard  $Z_L=0$ , and the equation (5.5) is represented as:

$$Z_{in} = jZ_0 \tan \beta l \quad (5.8)$$

It means we can design the input impedance as any reactance value from 0 to  $\infty$  by varying the line length. Where the point locates from the shorted end terminal by  $(2n+1)\lambda_g/4$ ,  $Z_{in}=\infty$ , and the circuit is opened at the point. Moreover, the point does by  $n\lambda_g/2$ ,  $Z_{in}=0$ , and the circuit is shorted. However, in this experiment, the efficiency is the maximum value near  $\lambda_g/4$ , and the minimum near  $\lambda_g/2$ . It is because the effect of the lead line length from the diode package end to the D-G line junction is so large that we cannot ignore it; the length would be about  $(2n+1)\lambda_g/4$ . The influence determined the rectifier circuit patterns and the diodes. Thus, once we optimized the D-G length, we will not need to change the length unless the diodes are changed.

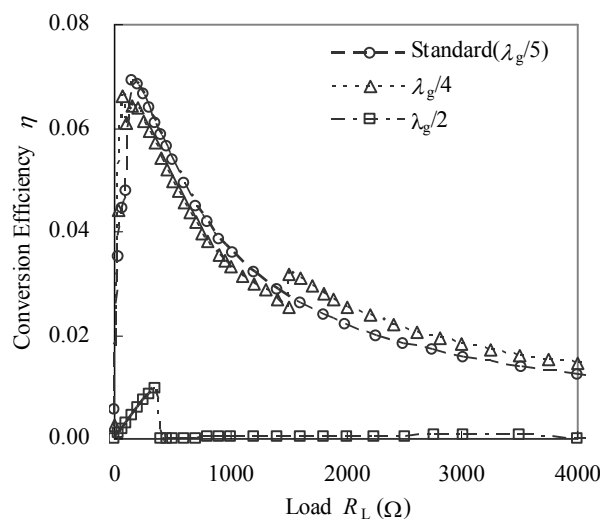


Figure 5.14 Load Characteristic related to D-G Length

### 5.2.7 Stub Length after Diode: $l_s$

The stub after diode was theoretically unnecessary because there is no AC effect before and after diode. However, in the research by the University of Kyoto, it was founded that there remained some AC effects. For remove the effects, the stub was needed as a filter. I considered it, and varied the stub length as a parameter with whittling away. In this experiment, I compared them by their open output voltages; it was enough to discuss the conversion efficiency. Figure 5.15 shows the result. As seen in this graph, the stub length was actually related to the conversion efficiency, and it said there reminded some AC effects. Moreover, while it fluctuated slightly, the output voltage decreases with increasing the stub length. As a result, although the length was one of the effective parameters, it was unnecessary in my rectifier circuit ( $l_s=0$ ).

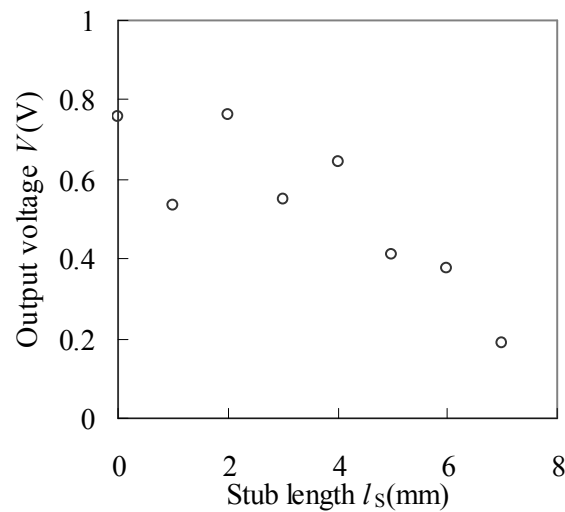


Figure 5.15 Relationship between Stub Length and Output Voltage

### 5.2.8 Output Transmission Line (OTL) Length: $l_{tl}$

The output transmission line (OTL) length is determined as  $l_{tl}=\lambda_g/4$  by the rectifier circuit designing (3.3.1). However, it was founded that we should treat the length as a variable parameter in recent researches;<sup>25</sup> it would depend on the inner capacitance element of the diode  $C_j$ . Thus I made some different patterns in the OTL length and experimented;  $l_{tl}=\lambda_g/8, 3\lambda_g/8$ .

Figure 5.16 show the influence from the difference in the length. From this graph, I can say the length is also one of the effective parameters and the conversion efficiency is the highest where  $l_{tl}=\lambda_g/4$  as the theory. However, with considering the researches, since the rectifier patterns might happen to follow the theory, we should experiment with the different patterns in the OTL length for confirming the conversion efficiency characteristic when we used other diode types.

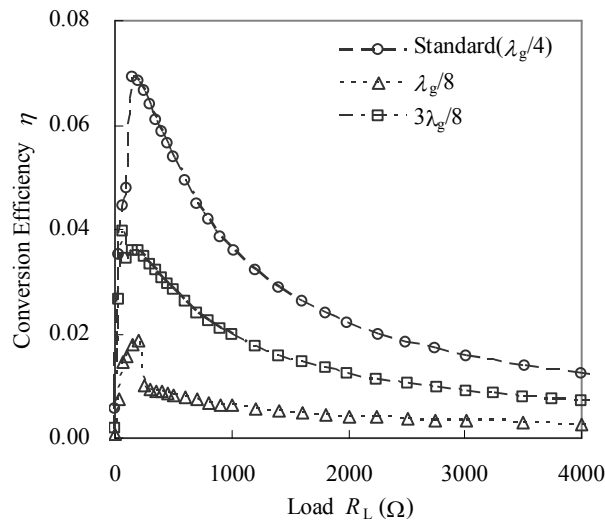


Figure 5.16 Load Characteristic related to OTL Length

### 5.2.9 Low Pass Filter (LPF) Shape: $W_C, l_C$

$W_C$  and  $l_C$  are the width and the length of the output LPF. Its equivalent circuit is a condenser connected in parallel (Figure 3.11), and its capacitance can be found by the equations (3.16-18). From the equations, the standard LPF capacitance  $C_{eq\_std}$  was about 1.33pF, and it was enough large to smooth output DC and to filter the reminded AC. For observing the effects of the LPF shape, I designed another LPF shape;  $W_C=25\text{mm}$ ,  $l_C=3\text{mm}$ , and  $C_{eq}=1.76\text{pF}$ .

Figure 5.17 shows the characteristics of two different LPF shapes. As seen in this figure, there are little difference of the conversion efficiency in the shape and the capacitance value when the LPF capacitance is enough large. As a result, the shape is not effective for developing the conversion efficiency, and it is free to design the size when the capacitance is enough large to fulfill its role.

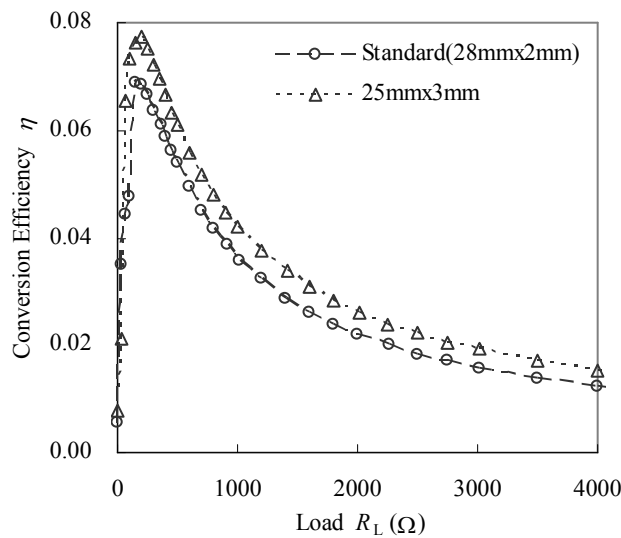


Figure 5.17 Load Characteristic related to LPF shape

### 5.2.10 Output Length: $l_{out}$

Since the output length was also not related to the conversion efficiency theoretically, I adopted the value of  $l_g=10\text{mm}$ , about  $3\lambda_g/8$ , for the design simplicity. However, if the RF element exists in the output line, the length would affect the efficiency. Thus, I surveyed the effect of the length  $l_{out}$  as well as  $W_g$  and  $l_g$ .

Figure 5.18 shows the result. From this, I can say the RF element reminded in the output line because this parameter has a great influence on the conversion efficiency. I discuss the effect as  $l_{in}$ .

Normally, it is ideal that the transmission length is  $n\lambda_g/2$  because the input impedance is represented as the load impedance for matching the circuit impedances. However, in this experiment, I connected the output to the load by BNC coaxial cable. The line length from the DC output feeding point of the rectifier circuit to the load is already about  $(4n+1)\lambda_g/8$ , and the total length become  $n\lambda_g/2$  with the output length of  $3\lambda_g/8$ . As a result, the efficiency reaches the maximum value at  $l_{out}=3\lambda_g/8$ . Furthermore, for resolving the RF effects in the output line, we need more effective filtering circuit for the harmful RF.

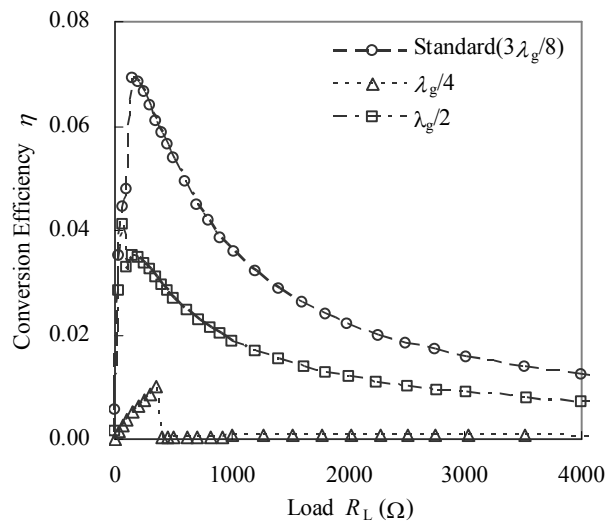


Figure 5.18 Load Characteristic related to Output Length

### 5.2.11 Redesign of Rectifier Circuit

Based on the above results, I redesigned the rectifier circuit. Table 5.3 shows the redesigned parameters.

Figure 5.19 shows the effect of redesigning. As a result, the conversion efficiency of the redesigned circuit reduced from the standard rectifier circuit. From this, they are not independent parameters, but related to each other in the conversion efficiency, and the pattern composed of the optimized parameters is not always optimized as a whole. It is because the RF elements exist in the parts before and after the diode where theoretically they do not, and it makes the simulation for the circuit characteristics difficult. Therefore, for improving the conversion efficiency of the rectifier circuit, I find that it is counts to design the rough circuit pattern with simulation and then optimize the parameters one-by-one.

**Table 5.3 Parameters of Redesigned Rectifier Circuit Pattern**

Parameters	Value / Product
$D$	1SS97 (NEC)
$C_0$ [pF]	33 (muRata-GRM42-6 SL 330J 50)
$W$ [mm]	2.83
$l_{in}$ [mm]	6.67 ( $\lambda_g/4$ )
$W_g$ [mm]	1.00
$l_g$ [mm]	6.67 ( $\lambda_g/4$ )
$W_S$ [mm]	-
$l_S$ [mm]	0
$l_{tl}$ [mm]	6.67 ( $\lambda_g/4$ )
$W_C$ [mm]	25.00
$l_C$ [mm]	3.00
$W_{out}$ [mm]	1.00
$l_{out}$ [mm]	10.00

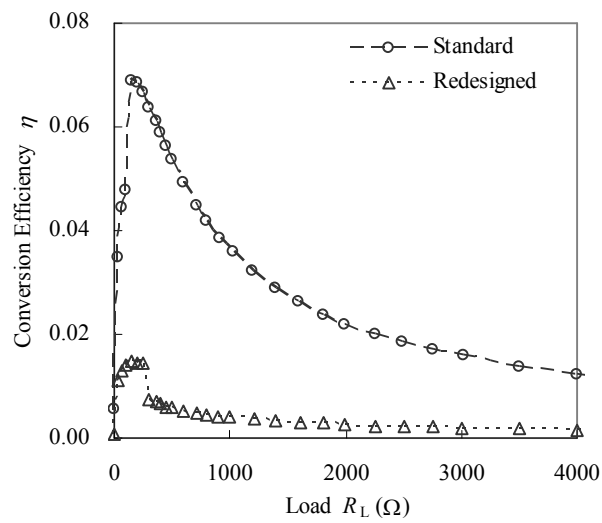


Figure 5.19 Load Characteristic before and after Redesigning

### 5.3 Rectenna Demonstration

I made rectennas by combining the antenna elements and the rectifier elements based on the above experimental results. The adopted antenna elements were the Leaf MSAs shown in Table 5.1, and the parameters of the rectifier circuit patterns were shown in Table 5.4.

**Table 5.4 Parameters for Rectenna Array**

Parameters	Value / Product
$D$	1SS97 (NEC)
$C_0$ [pF]	33 (muRata-GRM42-6 SL 330J 50)
$W$ [mm]	2.83
$l_{in}$ [mm]	6.67 ( $\lambda_g/4$ )
$W_g$ [mm]	1.00
$l_g$ [mm]	8.20
$W_s$ [mm]	-
$l_s$ [mm]	0
$l_{tl}$ [mm]	6.67 ( $\lambda_g/4$ )
$W_C$ [mm]	25.00
$l_C$ [mm]	3.00
$W_{out}$ [mm]	1.00
$l_{out}$ [mm]	10.00

#### 5.3.1 Combining Antenna with Rectifier

I connected the RF feeding point of the antennas to that of the rectifier circuit by the lead lines. They shared the ground by gluing their ground faces behind the face printed the patterns together. For the high-frequency circuits, it is important to cordon off as large ground sharing area as possible. In the experiments, I used the nonconductive adhesive for gluing. Thus, I applied the adhesive at the edge of the substrate, and slipped a piece of foil in between them inside of the gluing area.

The conversion efficiency of the antennas was 36% on an average, and that of the rectifier circuit 14% at a maximum with the load of 250 $\Omega$ . However, since the load resistance for this demonstration was about 33 $\Omega$ , the actual conversion efficiency was estimated to about 5%. Thus, the conversion efficiency of this rectenna was calculated as about 1.8% at a maximum. There might be a gap between the optimized input length and the actual optimal length from the section 5.2.4 because of feeding RF not with connectors but with lead lines directly. Therefore, the actual conversion efficiency of the rectennas guessed under 1.8%.



### 5.3.2 Parallel Connection of Rectenna

We can treat the rectenna elements as DC power supplies because the RF is converted to the DC by the diodes. Therefore, we can connect them each other in series and in parallel. The output voltage is increase with connecting them in series, and the output current does in parallel. By combining the method of the series connection and of the parallel one suitably according to the system, we can make the best use of the obtained power. We should prefer the parallel connection because of the report that the power combining loss with the parallel connections was smaller than with the series connection.<sup>26</sup>

As the explorative experiments before the main demonstration, I surveyed the effects of the series connection and the parallel one with the rectifier circuits consisted of the micro-strip lines. However, although I observed the combined power in parallel, I failed to obtain the power in series. From the results, I adopted the rectenna array pattern connecting the rectenna elements in parallel for the demonstration. Moreover, I assumed the adverse effects for DC by combining the different RF elements in phase because the RF elements existed in the rectifier output side from the section 5.2.10. Therefore I designed the pattern for all line lengths from the rectifier output feeding point to the combining point to equal. Figure 5.20 shows the rectenna array connecting four elements in parallel.

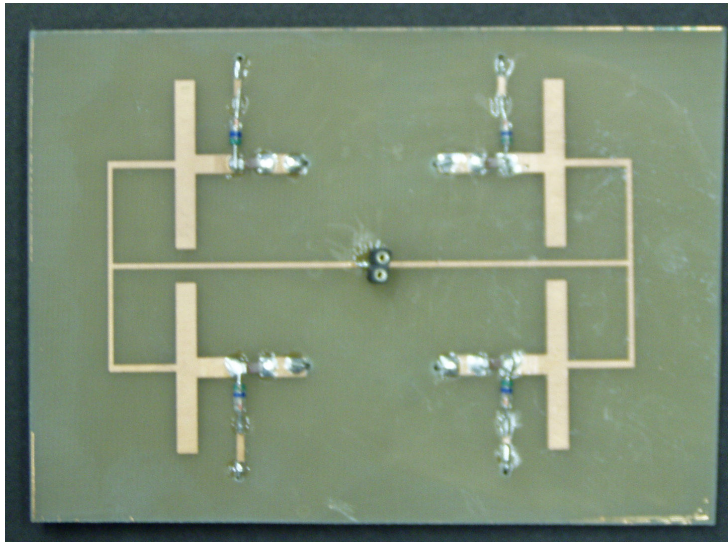


**Figure 5.20** Picture of Rectenna Array (Rectifier Face)

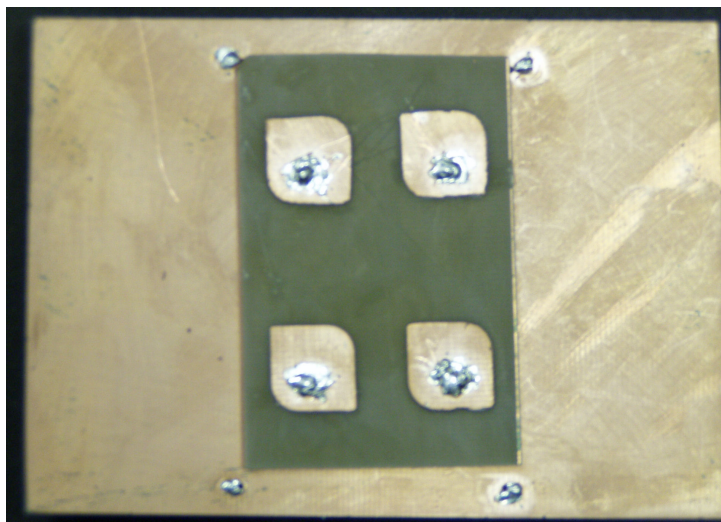


**Figure 5.21** Picture of Rectenna Array (Antenna Face)

### 5.3.3 Demonstration

I tested the demonstration for running the electric motor. The motor was installed on the ground and the rectennas were placed over the transmitting horn antenna. When the height from the aperture of the horn antenna to the rectenna array was 0~2cm, I confirmed the motor running.

In nature, the wave surface at the aperture of the horn antenna is not planate but orbiculate, and the electrical field is expressed as:

$$\left. \begin{aligned} E &= E_0 \sin \frac{\pi x}{a} \exp\left(-jk\sqrt{x^2 + c^2}\right) \\ c &= \frac{a}{2} \cot \frac{\alpha}{2} \end{aligned} \right\} \quad (5.9)$$

where the coordinate system is shown in Figure 5.22. For the simplicity of this problem, I assume the electric field, or the power  $P_0$  of 700mW supplied distribute uniformly on the aperture as a planate wave, and then the power  $P_L$  used by the motor is expressed as:

$$P_L = \eta_{MSA} \cdot \eta_{rect} \cdot P_{in} = \eta_{ant} \cdot \eta_{rect} \cdot \frac{S_{MSA}}{S_{horn}} P_0 \quad (5.10)$$

where  $\eta_{MSA}$  and  $\eta_{rect}$  are the conversion efficiencies of the antenna and the rectifier at the load resistance of  $30\Omega$ , and  $S_{MSA}$  and  $S_{horn}$  are the receivable area of the MSA and the aperture area of the horn antenna. By this equation,  $P_L$  was figured as 0.83mW where  $S_{MSA}=595[\text{mm}^2]$ ,  $S_{horn}=9020[\text{mm}^2]$ ,  $\eta_{MSA}=0.35$ ,  $\eta_{rect}=0.05$  at  $30\Omega$ . From this, although  $P_L$  was smaller than the minimum operating power of 1.2mW, we were able to operate the motor. I consider it is because the planar approximation of the wave surface at the aperture is little excessive and the power density is more large around the center of the aperture than I expected, and because, by connecting the rectifiers in parallel and sharing their voltages, the voltages of the diode increase averagely, the losses from  $V_f$  effects decrease, and then the rectifier conversion efficiency is improved.

Moreover, the motor was running continuously with rotating the rectenna array. As a result, I also confirmed the polarity-free characteristics of the Leaf MSAs.

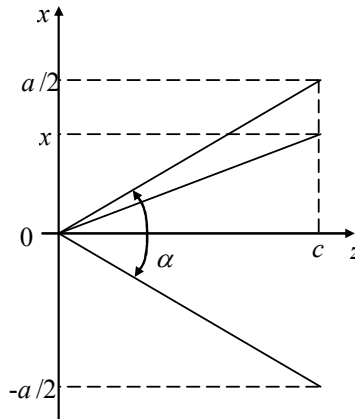


Figure 5.22 Coordinate System of Horn Antenna

# Chapter 6 Conclusions

This chapter shows the conclusions of my study, the perspectives and the issues in the future.

## 6.1 Conclusions

From my results, I establish the guideline for designing the self polarity-free MSA, and developed the polarity-free MSA with its conversion efficiency of 36% on an average, 33% at a minimum and 40% at a maximum. Moreover it is more effective than the unit of the multiple dipole antennas around all angles.

Secondly, I developed the rectifier patterns with the maximum conversion efficiency of 14% at the load resistance of  $250\Omega$ . Furthermore, I find the parameters of that do not affect the conversion efficiency in theory are very important because the RF elements remind in their elements before and after the diode; the type of the schotkky barrier diode  $D$ , the input length  $l_{in}$ , the length between the diode and the ground  $l_g$ , the stub length after the diode  $l_s$ , the input length  $l_{in}$ , the output transmission line length  $l_{tl}$ , the output length  $l_{out}$ . Moreover, they are not independent parameters, but related to each other in the conversion efficiency, and the pattern composed of the optimized parameters is not always optimized as a whole.

Lastly, I developed the rectenna array composed of four elements in parallel, and the elements consists of the Leaf MSAs with the efficiency of 36% on an average as the polarity-free antennas and the rectifier circuit with the maximum one of 14% at the load resistance of  $250\Omega$ . With this rectenna array and the power supply of 700mW by the horn antenna, I achieved the electrical motor operating at the height of 0~2cm from the aperture of the transmitting antenna.

## **6.2 Future Perspectives and Issues**

In my study, since I did not use the optimized substrate, the size of the rectifier circuit patterns was larger than that of the antennas. As the resolution, I was able to achieve a balance of their sizes with using the low dielectric constant substrate for the antenna to increase the size and the high one for the rectifier circuit to decrease.

Moreover, I designed the antennas by calculation based on the theory. However, I find there is still room for improvement in the position of the RF feeding point and the side length. In the future study, we should optimize the parameters with the analytical results from the computer simulations of the electromagnetic field, and actually confirm the improvement with the experiments.

It is desirable to apply the simulation to the rectifier circuit pattern designing. However, realistically it is difficult because the high-frequency properties vary greatly according to the component properties such as its type and its production lot. Furthermore, I find the adverse effects to the conversion efficiency from the RF elements existing before and after the diode. As the solutions, we need the insert of the low pass filters cutting the RF elements and the use of the diode with the high response speed, and then we will improve the rectifier conversion efficiency. In my experiments, I measured the rectifier characteristics with fixing the input power. However, we need to optimize the input power and the load resistance as variables for the rectifier conversion efficiency.

In addition, I achieved the parallel connection of the rectennas, but I failed to do the series connection. Hereafter, we should identify and address the cause. Furthermore, we should survey the effects of these conjunctive on the total conversion efficiency, and design the total system with the optimized conjunctive, the optimized input power and the optimized load.

With these improvements, we will install this system and demonstrate the microwave power supply for flying MAV.

# References

- <sup>1</sup> 小澤 亮二, “マイクロ波エネルギー伝送における移相制御と指向性,” 学士論文, 東京大学, Feb. 2005.
- <sup>2</sup> R. Ozawa, “Development of Microwave Energy Supply System,” Master thesis, University of Tokyo, Feb. 2007.
- <sup>3</sup> 小暮 裕明, “電磁界シミュレータで学ぶ ワイヤレスの世界,” CQ 出版社, Jun. 2001.
- <sup>4</sup> 太田 浩一, “電磁気学 I,” 丸善, Oct. 2000.
- <sup>5</sup> 平田 仁, “マイクロ波工学の基礎,” 日本理工出版会, Feb. 2004.
- <sup>6</sup> T. Yoo and K. Chang, “Theoretical and Experimental Development of 10 and 35 GHz Rectennas,” *IEEE Trans. Microwave Theory and Tech.*, Vol.40, No.6, Jun. 1992.
- <sup>7</sup> “アンテナハンドブック,” CQ 出版社, Feb. 1985.
- <sup>8</sup> 後藤 尚久, “図説・アンテナ,” (社)電子情報通信学会, Mar. 1995.
- <sup>9</sup> B. Strassner and K. Chang, “5.8-GHz Circularly Polarized Rectifying Antenna for Wireless Microwave Power Transmission,” *IEEE Trans. Microwave Theory and Tech.*, Vol. 50, pp. 1870-1876, Aug. 2002.
- <sup>10</sup> 阿部 英太郎, “マイクロ波,” 東京大学出版会, Mar. 1983.
- <sup>11</sup> <http://www.icom.co.jp/beacon/technical/antenna/005.html>
- <sup>12</sup> 羽石 操, 平澤 一紘, 鈴木 康夫, “小型・平面アンテナ,” (社)電子情報通信学会, Aug. 1996.
- <sup>13</sup> R. J. Gutmann and J. M. Borrego, “Power Combining in an Array of Microwave Power Rectifiers,” *IEEE Trans. Microwave Theory and Tech.*, Vol. MTT-27, pp. 958-968, Dec. 1979.
- <sup>14</sup> R. J. Gutmann and J. M. Borrego, “Solar power satellite rectenna design study: directional receiving elements and parallel-series combining analysis,” NASA Final Rep. NAS9-15453, Ch. 3, Dec. 1978.
- <sup>15</sup> 三宅 智之, 呉 南健, 雨宮 好仁, “マイクロ波送電に用いる整流素子の最適設計,” *Technical report of IEICE*, PE-95-8, pp7-12, Jul. 1997.
- <sup>16</sup> 谷村 佳則, “5.8GHz 用レクテナの開発,” 学士論文, 京都大学, Feb. 2002.
- <sup>17</sup> 山下 榮吉, “マイクロ波シミュレータの基礎,” (社)電子情報通信学会, Mar. 2004.
- <sup>18</sup> H. A. Wheeler, “Transmission-line properties of a strip on a dielectric Sheet on a plane,” *IEEE Trans. Microwave Theory and Tech.*, Vol. MTT-25, pp.631-647, 1977.
- <sup>19</sup> 小西 良弘, “マイクロ波回路の基礎とその応用,” 総合電子出版社, Aug. 1990.
- <sup>20</sup> 谷口 慶治, “マイクロ波電子回路 -設計の基礎-,” 共立出版, Mar. 2004.
- <sup>21</sup> 加藤 肇, 見城 尚志, 高橋 久, “図解・わかる電子回路 -基礎から DOS/V 活用まで-,” 講談社, Sept. 1995.
- <sup>22</sup> “Free-space microwave power transmission study-combined phase III and final report: Appendix

I,” Raytheon Company, NASA-CR-144151, Sept. 1975.

<sup>23</sup> J. O. Mcspadden, T. Yoo and K. Chang, “Theoretical and Experimental Investigation of a Rectenna Element for Microwave Power Transmission,” *IEEE Trans. Microwave Theory and Tech.*, Vol. 40, pp. 2359-2366, Dec. 1992.

<sup>24</sup> J. O. Mcspadden, L. Fan and K. Chang, “Design and Experiments of a High-Conversion-Efficiency 5.8GHz Rectenna,” *IEEE Trans. Microwave Theory and Tech.*, Vol. 46, pp. 2053-2060, Dec. 1998.

<sup>25</sup> 篠原 真毅, 岡田 寛, 三谷 友彦, 松本 紘, “マイクロ波エネルギー伝送用レクテナ整流回路のパラメータ最適化に関する研究,” 第24回宇宙エネルギーシンポジウム講演論文集 pp. 125-129, Mar. 2005.

<sup>26</sup> 三浦 健史, 篠原 真毅, 松本 紘, “マイクロ波電力伝送用レクテナ素子の接続法に関する実験的研究,” 電子情報通信学会論文誌 B, Vol. J82-B, No.7, pp.1374-1383, Jul. 1999.

**学会発表**

- (ア) 第 25 回 宇宙エネルギーシンポジウム, 神奈川, 3 月, 2006.  
“MAV 搭載用マイクロ波エネルギー受電レクテナシステム”
- (イ) 45<sup>th</sup> AIAA Aerospace Sciences Meeting and Exhibit, Reno, Nevada, Jan. 2007.  
“Power Transmission to a Micro Aerial Vehicle”

**学会誌掲載**

- 第 25 回 宇宙エネルギーシンポジウム 講演論文集, 2006.
- AIAA paper, 2007.



# Acknowledgements

I would like to express his sincerest gratitude to my advisor, Associate Professor Kimiya Komurasaki (Department of Advanced Energy, University of Tokyo) for his continuous and attentive guidance, support, discussion, and encouragement.

I would like to express my thanks to Professor Yoshihiro Arakawa (Department of Aeronautics and Astronautics, University of Tokyo) for his insightful advices.

I would like to express my gratitude to the members of Komurasaki Laboratory and Arakawa Laboratory for their intellectual and social contributions. Mr. Oda, Mr. Takayanagi, Mr. Ozawa, Mr. Ertel, Mr. Komatsu helped me while studying about the microwave power transmission together. Dr. Koizumi, Mr. Yokota gave me a lot of precious advice.

I am grateful to Associate Professor Naoki Shinohara (Research Institute for Sustainable Humanosphere, University of Kyoto) for his advice about the microwave power transmission.

Without any of these support, this thesis would not have been completed. Thank you.

Finally, I gave my special thanks to my family for their financial and mental support throughout my education and to all of the MIKAWA dormitory mates.